**Title**

*Tbx1* heterozygosity in the oligodendrocyte lineage has distinct effects on myelinated axons in the fimbria and on behaviors related to neurodevelopmental disorders in mice.

**Authors**

Anne Marie Wells, PhD[1,2], Takeshi Takano, PhD[2,3], Takaki Tanifuji, MD, PhD[2], Gina Kang, B.Sc.[2], Marisa Esparza, B.Sc.[2], Arumu Endo, MD.[2], Takeshi Hiramoto, PhD[2], Qian Shi, PhD[4], Manzoor A. Bhat, PhD[4], Noboru Hiroi, PhD[2, 4,5**]

[1]South Texas Medical Scientist Training Program (STX-MSTP), [2]Department of Pharmacology, [4]Department of Cellular and Integrative Physiology, [5]Department of Cell Systems and Anatomy, University of Texas Health Science Center, San Antonio, TX 78229, USA; [3]Tokyo Denki University, Saitama 350-0394, Japan

**ORCID:** 0000-0002-6846-5969

****Corresponding Author**
Noboru Hiroi, PhD
hiroi@uthscsa.edu
Department of Pharmacology
Department of Cellular and Integrative Physiology
Department of Cell Systems and Anatomy
University of Texas Health Science Center, San Antonio
Room 211B
7703 Floyd Curl Drive
San Antonio, TX 78229
+1 210 567 4169 (tel)

# of figures: 7
# of supplementary figures: 2
# of supplementary tables: 1

**Key Words**
*Tbx1*, *Nestin, Pdgfrα, Ng2, Cspg4,* 22q11.2 CNV, cognition, fimbria, axon development, myelination, hippocampus

**Acknowledgments**
The LifeCanvas device was purchased with generous donations by 10 scientists at UT Health San Antonio. We thank Dr. Bernice Morrow for providing *Tbx1*$^{+/flox}$ breeders, Ms. Monica D. Alarcon for technical assistance with EM analysis, and Dr. Lacey B. Sell for her help with MyleTracer software.

**Funding**

T. Takano, GK, ME, TH, and NH were supported by the National Institute of Health (R01MH099660). T. Tanifuji was supported by SENSHIN Medical Research Foundation and Uehara Memorial Foundation. QS and MAB were supported by the National Institute of Health (R01GM63074). AMW was funded by F30MH134482, UT Health San Antonio CTSA T32 (T32R004545), UT Health San Antonio Neuroscience T32 (T32NS082145), STX-MSTP (NIH T32GM113896/T32GM145432), and SfN NSP Fellowship (R25NS089462). The content is solely the responsibility of the authors and does not necessarily represent the official views of the National Institutes of Health.

**ABSTRACT**

The hemizygous deletion of human chromosome 22q11.2 leads to cognitive and social deficits, as well as psychiatric disorders. Constitutive deletion of *Tbx1*, a T-box transcription factor gene encoded within this chromosomal region, results in deficits in various cognitive and social behaviors and altered formation of oligodendrocytes, myelin, and myelinated axons in the fimbria of adult mice. Given that *Tbx1* is present in neonatal stem cells and oligodendrocytes, the present study was designed to test the hypothesis that *Tbx1* heterozygosity in the oligodendrocyte lineage contributes to behavioral phenotypes relevant to neurodevelopmental disorders and ultrastructural changes in myelinated axons in the fimbria. To this end, we conditionally induced *Tbx1* heterozygosity in the oligodendrocyte lineage in *Pdgfrα*Cre;*Tbx1*$^{+/flox}$ mice. This mouse line showed recombination in brain regions known to express *Pdgfrα*. Male *Pdgfrα*Cre;*Tbx1*$^{+/flox}$ mice performed better in spontaneous alternation in a T-maze than wild-type littermates at 1, but not 2 months of age; otherwise, mutant and wild-type littermates were indistinguishable in neonatal ultrasonic vocalization, peripubertal and postpubertal social interaction, novel object approach, anxiety-related behaviors in an elevated plus maze, and motor activity and thigmotaxis in an inescapable open field. The fimbria of male *Pdgfrα*Cre;*Tbx1*$^{+/flox}$ mice showed an increase in the number of myelinated axons in a range between ≥300 nm and <800 nm diameter and a decrease in the myelinated axons around 1,200 nm and 1,400 nm; the thickness of myelin was unchanged across all diameters. Our findings show that *Tbx1* heterozygosity in oligodendrocyte precursor cells or their progeny selectively improves spontaneous alternation and shifts the proportion of myelinated axons toward small- to medium-sized axons, suggesting that the compositional shift in axons in the fimbria induced by *Tbx1* heterozygosity in the oligodendrocyte lineage might underlie improved cognition relevant to neurodevelopmental disorders.

## INTRODUCTION

Cognitive and social impairments are predictors of mental illness(Hiroi & Yamauchi, 2019; Michelini et al., 2024). Infants and babies who are later diagnosed with autism spectrum disorder (ASD) exhibit delays and deviations in many elements of motor, social communication, and language development(Caravella & Roberts, 2017; Di Giorgio et al., 2021; Esposito et al., 2017; Miller et al., 2017; Miller et al., 2021; Northrup et al., 2021; Ozonoff et al., 2010; Ozonoff et al., 2014; Sung et al., 2022). Children who later develop full-scale symptoms of schizophrenia show delays in the development of social cognition, working memory, attention, and processing speed(Bora et al., 2014; R. C. Gur et al., 2014; Meier et al., 2014; Seidman et al., 2016; Sheffield et al., 2018), and after the onset of schizophrenia, these deficits remain as integral elements of schizophrenia(Johansson et al., 2020; Tschentscher et al., 2023).

These dimensional deficits of mental illness have genetic underpinnings. Copy number variations (CNVs) are deletions or duplications of up to a few million base pairs at specific chromosomal loci that include many protein-coding genes. Although each of CNVs is rare, occurring in <1% of individuals with a given mental illness, they have high odds ratios and penetrance rates for cognitive and social deficits(Kendall et al., 2017; Stefansson et al., 2014), and mental illnesses(Goh et al., 2024; Malhotra & Sebat, 2012; Marshall et al., 2017).

Carriers of the hemizygous deletion of human chromosome 22q11.2 exhibit cognitive, social, and emotional impairments from childhood (Hiroi et al., 2013; Hiroi & Yamauchi, 2019; Zinkstok et al., 2019) d(R. E. Gur et al., 2014) and are diagnosed, at high rates, with intellectual disability, ASD, schizophrenia, anxiety disorders, and attention-deficit hyperactivity disorder(Schneider et al., 2014; Zinkstok et al., 2019). However, how the more than 40 protein-encoding genes in 22q11.2 contribute to dimensional deficits and clinical diagnoses is poorly understood in humans. A few isolated cases of variants in human *TBX1*, a T-box transcription factor gene within the 22q11.2 CNV, are associated with ASD, schizophrenia, and intellectual disability without the 22q11.2 CNVs(Alghamdi et al., 2020; Alhazmi et al., 2022; Gong et al., 2001; Ogata et al., 2014; Paylor, Glaser, et al., 2006; Singh et al., 2022). However, as they are rare, the association between *TBX1* variants and mental illness lacks statistical reliability. Moreover, these patients carry variants in other single genes throughout the genome(Ogata et al., 2014), making it difficult to ascertain causality from these associations.

Deletion or overexpression of small chromosomal regions or single genes in mouse orthologs of human chromosome 22q11.2 provide a complementary approach and recapitulate specific behavioral features of 22q11.2 hemizygous deletions(Hiroi et al., 2012; Hiroi & Nishi, 2015; Hiroi et al., 2013; Hiroi & Yamauchi, 2019; Hiroi et al., 2005; Nishi & Hiroi, 2016). Constitutive overexpression of a few hundred kilobase pair segments of the mouse ortholog of 22q11.2 recapitulates social and cognitive deficits of 22q11.2 duplication(Hiroi et al., 2005; Suzuki, Harper, Hiramoto, Funke, et al., 2009), suggesting the existence of driver genes for distinct behavioral phenotypes.

*Tbx1* is one of the genes encoded in a 200kb 22q11.2 segment, overexpression and hemizygous deletion of which results in social behavior deficits, repetitive behavior, and prepulse inhibition deficits (Hiroi et al., 2005; Paylor, Glaser, et al., 2006). The heterozygous deletion of *Tbx1* alone results in defects in neonatal social communication(Hiramoto et al., 2011; Kato et al., 2021; Takahashi et al., 2016), postpubertal and adult social interaction(Hiramoto et al., 2011), social incentive learning(Hiramoto et al., 2025), and acoustic, but not non-acoustic, prepulse inhibition(Hiramoto et al., 2025; Paylor, Glaser, et al., 2006). Further, heterozygous deletion of *Tbx1* produces defects in spatial memory acquisition in the Morris water maze and in the simple discrimination and reversal phase of attentional set-shifting in adult mice(Hiramoto et

al., 2022). Virally produced overexpression of *Tbx1* in the hippocampus impairs the developmental maturation of working memory capacity(Boku et al., 2018).

In the post-embryonic mouse brain, TBX1 protein expression is enriched in stem cells in the hippocampal granule cell layer and subventricular zone (SVZ)(Hiramoto et al., 2011). When conditional *Tbx1* deficiency is induced in post-embryonic stem cells at P1–P5 but not P21–P25, mice have lower levels of social interactions(Hiramoto et al., 2023). Stem cells in the SVZ produce neural progenitor cells and oligodendrocyte precursor cells in the first neonatal week (Fuentealba et al., 2015; Rushing & Ihrie, 2016). Oligodendrocyte precursor cells generated in the SVZ migrate to the fimbria(Aguirre & Gallo, 2004; Menn et al., 2006). The fimbria of constitutive *Tbx1* heterozygosity in mice shows selective changes in the composition of myelinated axons, as well as a reduction of *Cspg4* (or *Ng2*)(Hiramoto et al., 2022), a molecule required for the maintenance and proliferation of oligodendrocyte precursor cells(de Vrij et al., 2019; Fruttiger et al., 1999). The fimbria contains major output and input projections from and into the hippocampus, and is critical for memory and cognition in rodents and humans(Gorny et al., 2002; Hodgetts et al., 2020; Liu et al., 2002; Olton & Feustle, 1981; Owen et al., 1991; White & McDonald, 2002). As *Tbx1* is also present in oligodendrocytes in the adult brain(Eom et al., 2024), the structural and behavioral phenotypes of constitutive and conditional *Tbx1* heterozygous mice might originate from neonatal stem cells, neuronal progenies, oligodendrocyte precursor cells, or oligodendrocytes.

In this study, we tested the hypothesis that *Tbx1* heterozygosity in the oligodendrocyte lineage from oligodendrocyte precursor cells to their progeny oligodendrocytes contributes to behavioral phenotypes and ultrastructural deficits of axons and myelin in the fimbria. We tested conditional *Pdgfrα*Cre;*Tbx1*$^{+/flox}$ mice for social communication during the neonatal period and a wide range of social, cognitive, anxiety-related, and motor behaviors at one and two months of age, as myelination starts around the second postnatal week and peaks around the fourth to fifth postnatal week in rodents(Downes & Mullins, 2014; Thompson et al., 2014). After behavioral testing, we examined myelinated axons in the fimbria by electron microscopy (EM). We found that *Tbx1* heterozygosity in the oligodendrocyte lineage partially affected cognitive behavior in an age-dependent manner and the composition of myelinated axons in the fimbria.

## METHODS

### Mice

All protocols for animal handling and use were approved by the Institutional Animal Care and Use Committee (IACUC) of the University of Texas Health Science Center at San Antonio (UTHSCSA) in accordance with National Institutes of Health (NIH) guidelines. Mice were housed in a vivarium with a standard light phase from 7 am to 9 pm).

C57BL/6J mice: We used 1- and 2-month-old male C57BL6/J mice (Jax #000664, Jackson Laboratory, Bar Harbor, ME) as stimulus mice for social interaction.

*Pdgfrα*Cre;*Tbx1*$^{+/flox}$ *mice*: To conditionally induce *Tbx1* heterozygosity in oligodendrocyte precursor cells, we chose a *Pdgfrα*Cre line that initiates Cre synthesis earlier than a *Cspg4*Cre line to better induce recombination in the oligodendrocyte lineage(Nishiyama et al., 1996). The *Pdgfrα*- promoter drives Cre-based recombination most robustly in oligodendrocyte precursor cells and their progeny oligodendrocytes but also in astrocytes, neurons, fibroblast-like cells, endothelial cells, vascular and leptomeningeal cells, and pericytes in the mouse brain(Beiter et al., 2022; Brandebura et al., 2018; Rivers et al., 2008; Sil et al., 2018).

We crossed hemizygous *Pdgfrα*Cre mice with *Tbx1*$^{+/flox}$ mice to generate *PdgfrαCre;Tbx1*$^{+/flox}$ mice. *PdgfrαCre* breeder mice (C57BL/6-Tg(*Pdgfrα*-Cre)1Clc/J; Jax #Brannn, Jackson Laboratory, Bar Harbor, ME) have a mixed C57BL/6J;C57BL/6N background. We backcrossed non-congenic *Tbx1*$^{+/flox}$ mice(Arnold et al., 2006) to C57BL/6J for more than 10 generations and confirmed that there was Cre-dependent recombination in a congenic *Tbx1*$^{+/flox}$ mice(Hiramoto et al., 2023). The genetic background of *Pdgfrα*Cre and *Tbx1*$^{+/flox}$ lines were mixed C57BL/6J;C57BL/6N and C57BL/6J, respectively. These two C57BL/6 substrains have many behavioral differences(Matsuo et al., 2010). To avoid the confounding effects of their unequal genetic backgrounds(Hiroi, 2018), we used only an F1 generation derived from crosses of the *Pdgfrα*Cre and *Tbx1*$^{+/flox}$ lines.

*Pdgfrα*Cre*;ROSA-tdTomato* mice: We crossed hemizygous *Pdgfrα*Cre mice (C57BL/6-Tg(*Pdgfrα*Cre)1Clc/J; Jax #013148, Jackson Laboratory, Bar Harbor, ME) with homozygous congenic *ROSA-CAG-tdTomato* mice (B6.Cg-*Gt(ROSA)26Sor*$^{tm14(CAG-tdTomato)Hze}$/J, Jax # 007914, Jackson Lab, Bar Harbor, ME) to generate *Pdgfrα*Cre*;ROSA-CAG-tdTomato* mice. This ROSA line expresses tdTomato in the hippocampus without the action of Cre ( http://connectivity.brain-map.org/transgenic/experiment/81560256)

We determined the genotypes of the mice using our previously published protocol with primers shown in **Table S1**. The sex of the mice was determined by inspection of their external genitalia.

### Whole Brain Tissue Clearing (Delipification) and Index Matching

We used the SHIELD and SmartBatch+ (LifeCanvas Sciences, Cambridge, MA) standard pipelines for preserving and electrophoretic clearing(Yang et al., 2024) to visualize tdTomato in the brains of *Pdgfra*Cre;ROSA-CAG-tdTomato mice. We performed transcardial perfusion of 1-month old mice with ice-cold 0.9% NaCl in $dH_2O$, followed by 4% paraformaldehyde (PFA) in phosphate-buffered saline (PBS). Brains were preserved using SHIELD as follows: perfused brains were 1) removed from the cranium and fixed in 4% PFA in PBS overnight at 4°C with gentle shaking; 2) incubated in SHIELD OFF solution ($dH_2O$ + SHIELD Buffer [cat#SH-Bf] + SHIELD Epoxy Buffer [cat#SH-Ex]) solution at 4°C with gentle shaking for 3 days; 3) incubated in pre-warmed SHIELD ON Buffer (cat#SH-ON) at 37°C for 1 day with gentle shaking; 4) incubated in the delipidation buffer (cat#DB) for 3 days at 45°C with gentle shaking. Final clearing by electrophoresis was performed with the SmartBatch+ device, with the delipidation buffer inside the clearing cup containing the samples and conduction buffer (cat#CB) for 30 h. Cleared brains were index-matched using a solution of 50% EasyIndex (RI = 1.52, cat#EI-500-1.52) + 50% $dH_2O$ with shaking at 37°C for 1 day, then 100% EasyIndex for one additional day until brains were transparent(Yang et al., 2024).

### Lightsheet Microscopy

We used a Zeiss Lightsheet 7 Microscope housed in the UTHSCSA Optical Imaging Core to perform volumetric lightsheet imaging of cleared *Pdgfrα*Cre;ROSA-CAG-tdTomato brains using a pair of 5×/0.1 focusing illumination objectives and a Fluar 2.5×/0.12 detection objective at identical settings. Image tiles were stitched together using Zeiss Zen Blue software (ver 3.4). 3D volume analysis was performed with Imaris (Oxford Instruments, ver 10.02). Peak intensity of the tdTomato signal was segmented, and volumetric measurements ($mm^3$) and peak intensities of the total volume (arbitrary units) were calculated for each volume in each mouse.

## Immunofluorescence

*Pdgfrα*Cre;ROSA-*tdTomato* mice were sacrificed at 1 month of age. Mice were deeply anesthetized using 4–5% isoflurane and perfused transcardially with 0.9% saline followed by 4% PFA. Brains were extracted and post-fixed in 4% PFA overnight at 4°C, followed by cryoprotection in glycerol overnight at 4°C. Coronal 60-μm thick sections were cut with a freezing microtome. For immunofluorescence labeling, sections were washed in 0.1 M PBS, blocked with 5% normal donkey serum in PBS, and incubated overnight at room temperature, as we described previously(Hiramoto et al., 2023; Hiramoto et al., 2022). We used well-validated primary rabbit anti-NG2 antibody (1:200, ab129051, Abcam) or a primary rabbit antibody against myelin basic protein (1:200, MBP, ab40390, Abcam) and Donkey anti-rabbit IgG-Alexa Fluor 488 (1:200, A21206, Invitrogen), together with a nuclear marker (DAPI,1:25,000, D3571, Invitrogen). Ng2 and MBP are markers of oligodendrocyte precursor cells and mature oligodendrocytes, respectively [42, 43][44, 45]. We captured images of sections that were mounted and cover-slipped with Vectashield® anti-fade mounting medium (H-1000) using a Keyence microscope (BZ-X800) microscope with BZX Hardware Module and Zeiss LSM 710 confocal microscope at the UT Health Optical Imaging Core.

### *Double staining of tdTomato with markers of oligodendrocytes*

We captured a series of coronal brain sections from *Pdgfrα*Cre*;ROSA-tdTomato* mice using a Keyence BZ-X800 microscope with BZX Hardware Module and a Zeiss LSM 710 confocal microscope at the UT Health Optical Imaging Core. We used the DAPI signal to identify the anatomical boundaries of landmark structures in each image, cross-matched with equivalent levels in the Allen Brain Atlas (Allen Reference Atlas – Mouse Brain [brain atlas]. Available from *atlas.brain-map.org*). We then used a color scale to represent the level of tdTomato intensity within the delineated anatomical boundaries.

## Behavioral Analysis

Male neonatal mice were tested for vocalization resulting from maternal separation at P8 and P12, followed by additional behavioral tests at 1 and 2 months of age, corresponding to peripubertal and post-pubertal periods, respectively; early signs of puberty begin around 1 month of age(Bronson et al., 2007). Because body weight can alter behavior in mice(Nakamura et al., 2021) and Pdgfrα regulates progenitor differentiation into adipocytes(Gao et al., 2018; Marcelin et al., 2017), we measured body weight at the beginning of behavioral tests. Our behavioral battery included reciprocal social interaction, novel object approach, spontaneous alternation in a T-maze, elevated plus maze, and locomotor activity and thigmotaxis in an inescapable open field(Boku et al., 2018; Harper et al., 2012; Hiramoto et al., 2011; Hiroi et al., 2005; Suzuki, Harper, Hiramoto, Funke, et al., 2009; Suzuki, Harper, Hiramoto, Sawamura, et al., 2009; Takahashi et al., 2016; Yamauchi et al., 2020b).

The order of the behavioral assays was based on the stress level; behaviors that occur in a home cage-like setting was given first (i.e., social interaction and novel object approach). T-maze and elevated plus maze tests permit choices and are thus considered less stressful than an inescapable open field. At least a one-day interval was provided between behavioral tests to reduce the likelihood of carryover effects(Hiramoto et al., 2025; Hiramoto et al., 2022; Paylor,

Spencer, et al., 2006), except for the T-maze, in which three different delays were given on three consecutive days.

Mice were assigned randomly to experimental groups and tested during the light phase. Experimenters were blinded to genotypes. Social interaction, novel object approach, and behaviors in the elevated plus maze were recorded using a Basler GigE camera and analyzed using Ethovision v18 software (Noldus Information Technology, Leesburg, VA). Spontaneous alternation in the T-maze was scored manually. Locomotor activity and thigmotaxis in an inescapable open field were analyzed by Med Associates Activity Monitor 7 Software (Fairfax, VT).

Ultrasonic vocalization Pups were tested for vocalization induced by maternal separation at postnatal days 8 and 12. A cage containing the mother and a litter was transferred to the test room 30 min before testing. Ultrasonic vocalization was recorded for 5 min by UltraSoundGate (Avisoft, Germany) connected to a computer equipped with Avisoft-RECORDER software (Avisoft, Germany) in a test chamber (18 cm long × 18 cm wide × 30 cm high). The sampling rate and lower cutoff frequency were set at 250 kHz (format, 16-bit) and 10 kHz, respectively. A frequency window from 15–150 kHz was used for analysis. Call detection was provided by an automatic threshold-based algorithm and a hold-time mechanism (hold time = 10 ms). Sonograms were inspected, and mechanical noises were eliminated from the analysis. We used the VocalMat software, which has the lowest false positive and false negative rates(Fonseca et al., 2021), to determine call types. This software typically detects only the most salient components of the harmonic call type and classifies this call type differently. As the harmonic call type is often affected in genetic mouse models of neuropsychiatric disorders(Hiramoto et al., 2011; Nakamura et al., 2021; Sakamoto et al., 2025; Takahashi et al., 2016), we manually inspected all call types and re-classified such cases as harmonic calls.

Reciprocal Social Interaction Test A test mouse and an age-matched unfamiliar C57BL/6J mouse as a stimulus subject were simultaneously placed in a cage (28.5 cm long × 17.5 cm wide × 12.5 cm high). Mouse behavior was recorded during two 5-min sessions with a 30-min interval between sessions. Video images were scored manually for affiliative and aggressive social interaction by a rater blinded to genotype. The following reciprocal social behaviors were scored by the duration of interaction (minimum of 1 s): aggressive (tail rattle, bite/kicks, sideway offense, boxing/wrestling), affiliative, non-aggressive (mount, pursuit, olfactory investigation, allogrooming, escape/leap), or passive (side-by-side, submissive). We analyzed the sum of time engaged in affiliative, active, and passive social interactions, but passive behavior was rarely seen in our experimental set-up (Hiramoto et al., 2023; Nakamura et al., 2021; Sakamoto et al., 2025; Yamauchi et al., 2020a).

Novel Object Approach A test mouse was placed in a cage (28.5 cm long × 17.5 cm wide × 12.5 cm high) with an empty, non-secured 50-mL Falcon tube (3 cm diameter × 8.5 cm long) lying on its side. Videos of mouse interactions with the tube were used to manually score approach behavior by two independent analysts blinded to genotype with an inter-rater reliability of >99%. Approach behavior was scored for olfactory or non-olfactory investigations with a minimum duration of 1 s. Time spent near the tube was also analyzed.

Spontaneous Alternation in a T-Maze A test mouse was placed in the start site of the long arm of a black plexiglass T-maze (21.5 cm long × 10.5 cm wide × 20.5 cm high) and allowed to enter the maze and explore either the left or right short arms (31 cm long × 10.25 cm wide × 20.5 cm high) of the cage. We imposed 0 s, 15 s, or 30 s interval delays to maze reentry for 10 trials, and

the three interval trials were given on three consecutive days. We manually scored the percentages of alternation and latency to reach the alternated and non-alternated arms.

Elevated Plus Maze Test Mice were placed in the center stage (5 × 5 cm) of the maze apparatus with four arms (30 × 5 cm) and permitted to explore two closed arms and two open arms extending from the center platform of the maze for 5 min. The maze was positioned 53 cm above the floor. The time spent in visits and the frequency of visits to the two open and two closed arms were analyzed.

Open Field Mice were placed in an open-field cage (27.3 cm × 27.3 cm × 20.2 cm; Med Associates, Fairfax, VT) and permitted to explore the cage for 30 min. We measured the distance and velocity of motor activity and duration of time spent in the center (19.05 cm × 19.05 cm central square) versus the margin of an open field, using the activity monitor software (Med Associates, Fairfax, VT).

**Electron Microscopy (EM)**

We prepared tissue for EM to characterize myelination in the fimbria of *Pdgfrα*Cre;*Tbx1*$^{+/flox}$ mice as we described previously(Hiramoto et al., 2022). After behavioral assays were completed at 1 and 2 months of age, 4–5-month-old male *Pdgfrα*Cre;*Tbx1*$^{+/flox}$ (N=3) and five control mice, including *Pdgfrα*Cre;*Tbx1*$^{+/+}$ (N=2), wild-type (WT);*Tbx1*$^{+/flox}$ (N=2), and WT;*Tbx1*$^{+/+}$ (N=1), were anesthetized with 4.5% isoflurane in a chamber, and anesthesia was maintained by a nose cone with 2.0% isoflurane. The animals were transcardially perfused with 120 mL of 0.9% saline followed by fixation with 120 mL of 0.1 M buffer (pH 7.4; cat#11653 Electron Microscopy Science, Hatfield, PA) with 2.5% sodium glutaraldehyde (cat#16310, Electron Microscopy Sciences, Hatfield, PA) and 2.5% paraformaldehyde (cat#19202, Electron Microscopy Sciences, Hatfield, PA). Brains were extracted and post-fixed in the same solution at 4°C for 7 weeks. The fimbria from the two hemispheres were obtained separately using a vibratome and placed in 0.1 M sodium cacodylate buffer overnight. Tissues were rinsed with 0.1 M sodium cacodylate buffer to remove aldehydes and placed in 2% osmium tetroxide solution ($OsO_4$; cat#19150, Electron Microscopy Sciences, Hatfield, PA) in 0.1 M sodium cacodylate buffer for 1 h. Tissues were dehydrated in a series of ethanol solutions and embedded in molds containing Polybed resin (Poly/Red® 812 Embedding media, cat#08791-500 Polysciences, Inc., Warrington, PA). We cut 100-nm sections and collected them on square 150-mesh copper grids (cat#7551C, Polysciences, Inc., Warrington, PA) and stained them with uranyl acetate (7 g in 100 mL deionized water)/Reynold's lead citrate (1.33 g lead nitrate,1.76 g sodium citrate in 30 mL triple-distilled water, 8 mL 1 N NaOH). Uranyl acetate stains membranous structures and structures containing nucleic acid; lead citrate binds to RNA-containing structures and the hydroxyl groups of carbohydrates.

Each fimbria section was viewed in the EM grid squares. Images were screened at 1,000× magnification. For each section, we used all grid images that contained fimbria tissue with round axons without wrinkles, folds, or tears in the sections. One image was captured at the center of each grid field at 20,000× magnification. Images were analyzed by MyelTracer(Kaiser et al., 2021). Only axons whose myelin was fully within the image were analyzed quantitatively.

We obtained multiple images for each animal from a section of the right and left hemispheres. The positions of sections sliced from the fimbria varied between the two hemispheres and did not necessarily match the two sides; in one case, only one hemisphere was available because of the accidental loss of a tissue slice. The number of images varied across tissue slices, resulting in

unequal image numbers. Many axons from each grid square and many grid squares from each hemisphere were analyzed for each animal. As the number of images and positions of each image varied between the two hemispheres and did not match between the two sides, the hemisphere could not be used as a replicate. Thus, we pooled data for each animal as a technical replicate; data points within and across images were technical replicates. As there was considerable variability in the data, we could not average the values for each animal. The averages of the total axon diameter per genotype were also not appropriate for this data set, as axon numbers differed between genotypes at specific axon diameters (≥300 nm to <400 nm; ≥1,200 nm to <1300 nm) (genotype × axon diameter range, $F(27,5880) = 6.336$, $P < 1.0 \times 10^{-4}$). Thus, generalized linear mixed models were used, as reported previously(Hiramoto et al., 2022). Data were assessed for the number of myelinated axons, the thickness of myelination, and the g-ratio along a 100 nm unit axon diameter. Data from different images and hemispheres were embedded in random models.

### Statistical Analysis

We used SPSS (v29.0.2.0 (20), IBM Corporation) to perform all statistical analyses. Among-group and between-group comparisons of the data were performed using analysis of variance (ANOVA) and Student's two-tailed t-test ($\alpha = 0.05$). We determined normality and homogeneity of variance using the Shapiro-Wilk test and Levene's homogeneity of variance test, respectively If either assumption was violated, we analyzed the data using a generalized linear mixed model, Kruskal Wallis tests, or Mann–Whitney U tests. The Greenhouse–Geisser correction was applied if sphericity was violated and the estimated epsilon was less than 0.75. If multiple tests were applied to a data set, the significance level was adjusted using the Benjamini–Hochberg correction, with a false discovery rate of 5%. We used GraphPad Prism software (v9; GraphPad Software, San Diego, CA) to generate all graphs.

### Data Availability

All data that support the findings and conclusions are provided within the article. All raw data and additional information are available upon request.

## RESULTS

*Localization of recombination in Pdgfrα*Cre*;ROSA-tdTomato* mice

We utilized a *Pdgfrα*Cre;*Tbx1*$^{+/flox}$ mice to initiate the conditional deletion of *Tbx1* in oligodendrocyte precursor cells. To assess the extent of *Pdgfrα*Cre-mediated recombination throughout the brain, we employed a tissue clearing technique (SmartBatch+) and conducted lightsheet microscopy to visualize the 3D volume of tdTomato signals in the brains of *PdgfrαCre*;ROSA-tdTomato mice (**Figure 1A**). The highest levels of tdTomato expression were observed in a pair of arch-shaped structures located along the lateral and third ventricles. Additionally, clusters of tdTomato signals were detected on the ventral surface of the posterior brain, while lower levels of signals were detected throughout other regions.

To further delineate the localization of tdTomato signals in *PdgfrαCre*;ROSA-tdTomato mice, we analyzed a series of coronal sections from a distinct cohort of *Pdgfrα*Cre;ROSA-tdTomato mice at one month of age (**Figure 1B–H**). The most prominent tdTomato signal was identified in the choroid plexus within the lateral ventricle. Robust tdTomato signals weren also present in the striatum, neocortex, hippocampal granule cell layer, and olfactory tubercle. This expression pattern driven by the *Pdgfrα* promoter aligns with previously reported distributions of *Pdgfrα* mRNA and protein, as well as recombination activity associated with the *Pdgfrα* promoter in the mouse brain (Allen Brain Atlas, 2017; Nait Oumesmar et al., 1997; Zhu, Bergles, et al., 2008; Zhu, Hill, et al., 2008).

*Initiation of Tbx1 heterozygosity in oligodendrocyte precursor cells has no detectable behavioral effects.*

Constitutive *Tbx1* heterozygous mice are impaired in 1) neonatal social communication as early as P7(Hiramoto et al., 2011; Kato et al., 2021; Takahashi et al., 2016), 2) postpubertal and adult social behaviors(Hiramoto et al., 2011; Hiramoto et al., 2025), 3) adult working memory/cognitive flexibility in a T-maze and attentional set shifting(Hiramoto et al., 2011; Hiramoto et al., 2022), and 4) affect-related behaviors in an inescapable open field, but not in an elevated plus maze(Hiramoto et al., 2011). To determine how *Tbx1* heterozygosity in oligodendrocyte precursor cells and their progenies contributes to behavior, we first measured the differences among the three control mice: *Pdgfrα*Cre;*Tbx1*$^{+/+}$, WT;*Tbx1*$^{+/flox}$, and WT;*Tbx1*$^{+/+}$. There was no significant difference among the controls (data not shown); therefore, we collapsed all the control genotypes into a single control group (named o*Tbx1*$^{+/+}$) for comparison with *Pdgfrα*Cre*;Tbx1*$^{+/flox}$ (named o*Tbx1*$^{+/-}$)

The rate of growth could affect behavior; *Pdgfrα*Cre;*Tbx1*$^{+/flox}$, termed o*Tbx1*$^{+/-}$ mice, may be delayed in development, and their phenotypes could reflect an earlier point in development compared to their wild-type littermates (i.e., o*Tbx1*$^{+/+}$). However, neonatal o*Tbx1*$^{+/+}$ and o*Tbx1*$^{+/-}$ mice had indistinguishable increases in body weights (**Figure S1**).

Constitutive *Tbx1*$^{+/-}$ mice exhibit various neonatal, peri-adolescent, and postnatal behavioral phenotypes(Hiramoto et al., 2011; Takahashi et al., 2016). Therefore, we tested mice for neonatal ultrasonic vocalization on P8 and P12–P13 and performed additional tests with

peripubertal (1 month) and postpubertal, preadult (2 months) mice with 1–2 day intervals between tasks to mitigate potential carryover effects of prior testing(Paylor, Spencer, et al., 2006). We found no differences among o*Tbx1*$^{+/-}$ pups in the number, percentage, and duration of various neonatal vocal call types on P8 and P12 (**Figure 2A–C**).

At 1 and 2 months of age, mice were tested sequentially for social interaction, novel object approach, spontaneous alternation in a T-maze, anxiety-related behavior in an elevated plus maze, and locomotor activity and thigmotaxis in an inescapable open field. The o*Tbx1*$^{+/-}$ mice and o*Tbx1*$^{+/+}$ mice were indistinguishable in social interaction (**Figure 3A**) and the novel object approach (**Figure 3B**). In a T-maze, o*Tbx1*$^{+/-}$ mice, at 1 month of age, had better spontaneous alternation rates at the longest delay (**Figure 4A**); otherwise, o*Tbx1*$^{+/+}$ and o*Tbx1*$^{+/-}$ mice were indistinguishable in the rates of spontaneous alternation at 2 months of age and in latencies to correct choices at 1 and 2 months of age (**Figure 4B–D**).

The two genotypes were indistinguishable in the percentage of time spent in open arms (**Figure 5A**) and visits to open arms (**Figure 5B**) of the elevated plus maze.

We evaluated their motor activity and anxiety-related behavior in the stressful, open-field task(Misslin et al., 1982; Zhu et al., 2007) where there is no chance to escape to closed arms. In this task, o*Tbx1*$^{+/-}$ and o*Tbx1*$^{+/+}$ mice were indistinguishable in distance travelled at 1 month or 2 months of age (**Figure 6A,B**) and time spent in the margin zone (**Figure 6C,D**).

While conditional *Tbx1* heterozygosity in the oligodendrocyte cell lineage resulted in improved spontaneous alternation, this phenotype is opposed to the impaired spontaneous alternation of constitutive *Tbx1* heterozygous mice (Hiramoto et al., 2011; Hiramoto et al., 2022). Moreover, this conditional *Tbx1* heterozygosity did not recapitulate the altered neonatal vocalizations, peripubertal or postnatal social interaction deficits, or heightened responses to a novel, non-social object seen in constitutive *Tbx1* heterozygous mice.

*Tbx1 heterozygosity initiated in oligodendrocyte precursor cells alters the proportions of the diverse sizes of myelinated axons but does not affect myelin thickness.*

Constitutive *Tbx1* heterozygosity selectively alters the ultrastructure in the fimbria. There is a higher proportion of 200–600 nm myelinated axons and a lower proportion of axons ≥700 nm and <1,200 nm. Further, the 700–1,500 nm axons have a thicker myelin sheath, and there are no larger myelinated axons(Hiramoto et al., 2022).

We determined whether these ultrastructural alterations were recapitulated in o*Tbx1*$^{+/-}$ mice with conditional *Tbx1* heterozygosity in the oligodendrocyte lineage. Densely packed axons were present in the fimbria (**Figure 7A**). To determine relative myelin thickness, we compared the ratio of the inner axon diameter to the outer fiber diameter (i.e., the g-ratio) (**Figure 7B**). As was the case with constitutive *Tbx1* mice, the g-ratio in o*Tbx1*$^{+/flox}$ mice plateaued at ~0.8, the ratio for optimal signal conductance in the brain (Chomiak & Hu, 2009). However, it did not differ between o*Tbx1*$^{+/-}$ mice compared to o*Tbx1*$^{+/+}$ mice over the entire range of axon diameters.

As the g-ratio does not indicate the size diameter variations of axons, we determined the number and proportion of axons of different diameters. The fimbria of o*Tbx1*$^{+/-}$ mice had more axons ≥ 300 nm and <800 nm but fewer axons >1,200 nm and <1,500 compared to o*Tbx1*$^{+/+}$ mice (**Figure 7C**). As a result, the curve for the relative proportions of axon diameter sizes (y-axis) versus the axon diameter (x-axis) shifted to the left in o*Tbx1*$^{+/-}$ mice, compared to o*Tbx1*$^{+/+}$ mice (**Figure 7D**). Consistent with g-ratios, the myelin thickness was indistinguishable between

the o*Tbx1*$^{+/-}$ mice and o*Tbx1*$^{+/+}$ mice for all axon diameters (**Figure S2**). Thus, conditional *Tbx1* heterozygosity in the oligodendrocyte precursor cells selectively shifted the relative proportion of small to medium myelinated axons in the fimbria but did not affect myelin thickness.

In sum, conditional *Tbx1* heterozygosity in the oligodendrocyte lineage shifted the proportion of myelinated axons to smaller sizes, but had no effect on the thickness of myelin in the fimbria.

## DISCUSSION

In this study, we aimed to determine the contribution of *Tbx1* heterozygosity in oligodendrocytes to the behavioral and ultrastructural phenotypes of constitutive *Tbx1* heterozygous mice. We previously found that constitutive *Tbx1* heterozygosity alters the composition of myelinated axons in the fimbria, a major connection fiber of the hippocampus, and these mice have deficits in neonatal social communication and post-pubertal social and cognitive behavior and heightened anxiety-related behavior(Hiramoto et al., 2011; Hiramoto et al., 2022; Kato et al., 2021; Takahashi et al., 2016). Induction of *Tbx1* heterozygosity in neonatal stem cells recapitulates some of the behavioral phenotypes of constitutive *Tbx1* heterozygosity in mice (Hiramoto et al., 2023). Neonatal stem cells in the lateral subventricular zone generate neurons and oligodendrocytes during the neonatal period (Fuentealba et al., 2015; Redmond et al., 2019; Rushing & Ihrie, 2016). Oligodendrocytes generated in the subventricular zone migrate postnatally to myelinate the fimbria(Aguirre & Gallo, 2004; Menn et al., 2006).

To determine whether induction of *Tbx1* heterozygosity in oligodendrocyte precursor cells recapitulates the behavioral and ultrastructural phenotypes of constitutive *Tbx1* heterozygosity, we crossed *Pdgfrα*Cre mice with congenic *Tbx1*$^{+/flox}$ mice to generate o*Tbx1*$^{+/-}$ (i.e., *Pdgfrα*Cre;*Tbx1*$^{+/flox}$) mice. We measured a wide range of social, cognitive, anxiety-related, and motor behaviors, as well as the ultrastructural composition of myelin and axons in the fimbria. *Tbx1* heterozygosity in the oligodendrocyte lineage selectively recapitulated the shifted axon sizes in the fimbria of constitutive *Tbx1* heterozygous mice. On the other hand, although o*Tbx1*$^{+/-}$ exhibited improved rates of spontaneous alternation with a higher cognitive load after a 30 s delay at 1 month of age, indicating a heightened capacity of working memory and cognitive flexibility, this was opposite to the impaired spontaneous alternation of constitutive *Tbx1* heterozygous mice. If this phenotype is not due to a stochastic event among the many tasks tested, it is consistent with the hypothesis that the ultimate phenotype reflects the sum of all contributory and opposing effects (Hiroi, 2018; Hiroi et al., 2013). Finally, other phenotypes of constitutive *Tbx1* heterozygosity were absent in o*Tbx1*$^{+/-}$ mice, including 1) neonatal social communication, 2) pubertal or postpubertal responses to social or non-social stimuli, 3) anxiety-like behaviors in an elevated plus maze and thigmotaxis, o*Tbx1*$^{+/-}$ mice 1) and 2) moved more in an inescapable open field(Hiramoto et al., 2011; Takahashi et al., 2016), suggesting that Tbx1 in the oligodendrocyte lineage does not have a significant impact on these phenotypes. Thus, *Tbx1* in neonatal stem cells might have the principal effect on the final phenotype (Hiramoto et al., 2023).

Taken together with our observation that *Tbx1* heterozygosity initiated in neonatal (P1–P5) stem cells but not postnatal/adult (P21–P25) stem cells recapitulate social and cognitive deficits of constitutive *Tbx1* heterozygous mice (Hiramoto et al., 2023), the present results delineate the role of *Tbx1* in neonatal stem cells and oligodendrocyte precursor cells and their progenies and indicate that *Tbx1* in oligodendrocyte precursor cells or their progenies only partially contributes to a set of phenotypes of constitutive *Tbx1* heterozygosity.

Several interpretative limitations warrant consideration. The general absence of phenotypes could be due to the high mortality of o*Tbx1*$^{+/-}$ litters. This selection might have biased our sample toward mice that were less affected by or recovered more quickly from the effects of this mutation. Among male pups born in the breeder colony, only 31% and 24% survived up to P7 and 2 months of age, respectively. However, two lines of evidence do not support this possibility. First, more mice were alive during the neonatal period than at 1 and 2 months of age, but neonatal vocalization on P8 and P12 was normal. Second, nestinCreERT;*Tbx1*$^{+/flox}$ litters have a similarly high mortality rate, but have more profound behavioral deficits (Hiramoto et al., 2023).

We cannot rule out the possibility that the conditional *Tbx1* heterozygosity was incomplete. The *Pdgfrα* promoter induces near complete recombination in oligodendrocyte precursor cells, and their labels persist in their mature progeny oligodendrocytes (Kang et al., 2010; O'Rourke et al., 2016); however, this promoter may be weaker in some cells, resulting in incomplete recombination (Tripathi et al., 2010).

A limitation of our study is that the constitutive *Tbx1* heterozygous mice had a congenic C57BL/6J background, whereas the F1 background of the o*Tbx1*$^{+/-}$ heterozygous mice was C57BL/6J and C57BL/6N, which was derived from the genetic background of the *PdgfrαCre* mice. C57BL/6J and C57BL/6N differ in baseline values in a wide range of behaviors(Matsuo et al., 2010; Simon et al., 2013). In the F1 generation we studied, mutant and WT littermates do not have skewed, biased distributions of alleles from C57BL/6J and C57BL/6N(Hiroi, 2018). Nonetheless, given that mutant mice with a C57BL/6N genetic background often have no or few behavioral phenotypes(Hiroi, 2018), including mouse models of 22q11.2 hemizygosity(Saito et al., 2020), 16p11.2 hemizygosity (Arbogast et al., 2016), and 15q13.3 hemizygosity (Fejgin et al., 2013), it is possible that the phenotype-suppressing C57BL/6N alleles affected our results.

The fimbria of o*Tbx1*$^{+/-}$ mice had more axons of ≥300 nm and <800 nm diameter and fewer axons of ≥1,200 nm and <1,500 nm diameter than o*Tbx1*$^{+/+}$ mice. This was similar to the increase in axons of ≥200 nm and <400 nm and the decrease in axons of ≥700 nm and <1,700 nm axons in constitutive *Tbx1* heterozygous mice(Hiramoto et al., 2022). The medium-size axons of constitutive *Tbx1* heterozygous mice have increased myelin thickness and lack large (≥1,700 nm) myelinated axons in the fimbria(Hiramoto et al., 2022), but these characteristics were absent in o*Tbx1*$^{+/-}$ mice. This selective change in the axon phenotype could result from a widespread activities of the *Pdgfrα* promoter in many cell types and regions. Although *Pdgfrα*Cre induces recombination in oligodendrocyte precursor cells, it also triggers recombination in neurons, astrocytes, pericytes, ependyma, perivascular mesenchymal cells, and other cells (Beiter et al., 2022; Brandebura et al., 2018; Kang et al., 2010; Komitova et al., 2009; Nait Oumesmar et al., 1997; Rivers et al., 2008; Sil et al., 2018). *Tbx1* heterozygosity in neurons might underlie the shift in the axonal composition of neurons. Similarly, the correlation between altered spontaneous alternation and the increased proportion of small-to-medium myelinated axons in the fimbria does not indicate causality by oligodendrocyte precursor cells. *Pdgfra*Cre-induced recombination could have affected phenotypes through other cell types and their progenies in other brain regions. More work is needed to determine how *Tbx1* in various cell types affects phenotypes.

Large-scale human brain imaging studies show alterations in the white matter in CNV carriers(Kochunov et al., 2020; Thompson et al., 2020), as well as idiopathic cases of ASD and schizophrenia(Kelly et al., 2018; Koshiyama et al., 2020). The fornix/fimbria is a region that shows robust white matter alterations. Moreover, carriers of hemizygous deletion of 22q11.2 have an altered white matter in the fornix/fimbria (Villalon-Reina et al., 2020) and volume alterations of many brain regions(Ching et al., 2020; Sonderby et al., 2021; Sun et al., 2020). Together with our previous observations that *Tbx1* heterozygosity during embryonic neurogenesis (Hiramoto et al., 2025) and in neonatal stem cells (Hiramoto et al., 2023) likely contribute to volume alterations of specific brain regions and social and cognitive deficits (Hiramoto et al., 2025), respectively, the present results that *Tbx1* heterozygosity in oligodendrocyte precursor cells has only limited impacts on phenotypes delineate the extent to which *Tbx1* contributes to the behavioral and structural phenotypes of 22q11.2 hemizygosity through its expression in different cell types.

**Figure legends**

**Figure 1. A.** A representative lightsheet image of the brain of a 1-month-old male *Pdgfrα*Cre;ROSA-tdTomato_ mouse following SmartBatch+ tissue clarification. N = 3. **B-D**. tdTomato expression in 1-month-old *Pdgfrα*Cre;ROSA-tdTomato mice is shown against blue DAPI signals at the levels of the anterior striatum (**B**), middle striatum (**C**), posterior striatum/fimbria (**D**), the anterior lateral ventricle (**E**), middle lateral ventricle (**F**), hippocampal granule cell layer (**G**), and fimbria (**H**). ChPx, choroid plexus; LV, lateral ventricle; Str, striatum; Sept, septum; CC, corpus callosum; CTX, cortex; HGCL, hippocampal granule cell layer; fmb, fimbria; SVZ, subventricular zone. N = 3.

**Figure 2**. The number (**A**), proportion (**B**), and duration (**C**) (mean ± standard error of the mean [SEM]) of 12 call types emitted on postnatal day (P) P8 and P12. As the assumption of normality was violated in many cases, we used the Mann-Whitney U test. The Benjamini–Hochberg method adjusted the significance at the false detection rate of 5%. **Inset in A**: The total number of ultrasonic vocalizations (mean ± SEM ) emitted at P8 and P12. The two genotypes did not differ for any call type or at any neonatal period. Ha, harmonic; Sd, step-down; Sh, short; Df, down frequency modulation; Uf, up frequency modulation; Ts, two steps, Fl, flat; Ch, chevron; Co, complex; Su, step-up, Ms, multiple-steps; Rc, reverse chevron. o*Tbx1*$^{+/+}$ mice, N = 27; o*Tbx1*$^{+/-}$ mice, N = 11 on P8; o*Tbx1*$^{+/+}$ mice, N = 30; o*Tbx1*$^{+/-}$ mice, N = 12 on P12.

**Figure 3. Interaction with social and non-social stimuli. A**) Social interaction. The o*Tbx1*$^{+/-}$ (*Pdgfrα*Cre;*Tbx1*$^{+/flox}$) mice and o*Tbx1*$^{+/+}$ mice did not differ in the amount of time (mean ±SEM) spent in affiliative social interaction (1 month, genotype, F(1, 72) = 0.1118, p = 0.739; genotype × session, F(1, 72) = 0.262, p = 0.6102: 2 months, genotype, F(1, 58) = 0.00547, p = 0.9413; genotype x session, F(1, 58) = 1.2175, p = 0.2744). o*Tbx1*$^{+/+}$ mice, N = 27; o*Tbx1*$^{+/-}$ mice, N = 11 at 1 month; o*Tbx1*$^{+/+}$ mice, N = 21; o*Tbx1*$^{+/-}$ mice, N = 10 at 2 months. **B**) Approach to a novel, non-social object. The two genotypes did not differ in the amount of time spent in affiliative social interaction (1 month, genotype, F(1, 70) = 2.2507E-05, p=0.9962; genotype × session, F(1, 70) = 1.0305, p = 0.31354: 2 months, genotype, F(1, 58) = 0.11634, p = 0.7342; genotype × session, F(1, 58) = 0.0821, p = 0.77545). o*Tbx1*$^{+/+}$ mice, N = 26; o*Tbx1*$^{+/-}$ mice, N = 11 at 1 month; o*Tbx1*$^{+/+}$ mice, N = 21; o*Tbx1*$^{+/-}$ mice, N = 10 at 2 months.

**Figure 4. Spontaneous alternation in a T-maze.** Compared to male o*Tbx1*$^{+/+}$ (N = 20) mice, male o*Tbx1*$^{+/-}$ (N = 10) performed better in the percentage of correct spontaneous alternations (mean ±SEM) at the most extended delay (30 s) in a T-maze at 1, but not 2 months of age (**A**, % alternation, 1 month, genotype, F(1, 96) = 4.66, p = 0.0333, genotype × delays F(2,96) = 3.1509, p = 0.0473; 2 months, genotype, F(1, 81) = 2.047, p = 0.1564; genotype × delays F(2, 81) = 0.2439, p = 0.7841). o*Tbx1*$^{+/-}$ mice showed higher levels of alternations at 30 sec delay, compared to o*Tbx1*$^{+/+}$ mice, as determined by the Mann-Whitney test (**, p =0.0081). **B**) The two groups did not differ in the latency to correct choices in the T-maze (1 month, genotype, F(1, 96) = 2.181, p = 0.1430, genotype × delays F(2, 96) = 2.058, p = 0.1332: 2 months, genotype, F(1, 81) = 1.1135, p = 0.2944; genotype × delays F(2, 81) = 2.5825, p = 0.0817).o*Tbx1*$^{+/+}$ mice, N = 24; o*Tbx1*$^{+/-}$ mice, N = 10 at 1 month; o*Tbx1*$^{+/+}$ mice, N = 20; o*Tbx1*$^{+/-}$ mice, N = 9 at 2 months.

**Figure 5. Anxiety-related behavior in an elevated T-maze.** The o*Tbx1*$^{+/-}$ mice and o*Tbx1*$^{+/+}$ mice did not differ in the relative amount of time (mean ±SEM) in open arms of an elevated plus maze (**A**, 1 month, U = 100, p = 0.3440; 2 months, U = 98, p = 0.9483) or frequency of visits to an open arms of an elevated plus maze (**B**, 1 month, t(32) = 1.7412, p = 0.0912; 2 months, t(28)

= 0.5925, p = 0.5583). o*Tbx1*$^{+/+}$ mice, N = 23; o*Tbx1*$^{+/-}$ mice, N = 11 at 1 month; o*Tbx1*$^{+/+}$ mice, N = 20; o*Tbx1*$^{+/-}$ mice, N = 10 at 2 months.

**Figure 6. Motor activity and thigmotaxis.** o*Tbx1*$^{+/+}$ mice and o*Tbx1*$^{+/-}$ mice traveled indistinguishable distance at 1 month and 2 months of age (**A**, 1 month, genotype, F(1, 198) = 0.6314, p = 0.4278; genotype × time, F(5, 198) = 0.9551, p = 0.4466: **B**, 2 months, genotype, F(1, 28) = 0.0242, p = 0.87739; genotype × time, F(3.66, 102.485) = 0.5389, p = 0.69188). The Greenhouse–Geisser correction was applied, as sphericity was violated and the estimated epsilon was less than 0.75. o*Tbx1*$^{+/+}$ and o*Tbx1*$^{+/-}$ mice equal amounts of time in the margin zone (i.e., thigmotaxis) of the inescapable open field at 1 and 2 months of age (**C**, 1 month, genotype, F(1, 198) = 0.2009, p = 0.6545; genotype × time, F(5,198) = 2.1516, p = 0.0609: **D**, 2 months, genotype, F(1, 168) = 0.08912, p = 0.7657; genotype × time, F(5, 168) = 0.9880, p = 0.4267). o*Tbx1*$^{+/+}$ mice, N = 24; o*Tbx1*$^{+/-}$ mice, N = 11 at 1 month; o*Tbx1*$^{+/+}$ mice, N = 20; o*Tbx1*$^{+/-}$ mice, N = 10 at 2 months.

**Figure 7. EM analysis of myelinated axons. A.** Representative EM images of axons in the fimbria at 20,000× magnification. +/+, o*Tbx1*$^{+/+}$; +/-, o*Tbx1*$^{+/-}$. Scale bar = 1,600 nm. **B**. G-ratios plotted against axon diameters for 4423 and 2317 axons in 5 o*Tbx1*$^{+/+}$ mice and 3 o*Tbx1*$^{+/-}$ mice, respectively. All axons with closed myelin sheaths were analyzed using MyelTracer. The reciprocal function best fits the data distributions. G-ratios increased as a function of axon diameter (o*Tbx1*$^{+/+}$, $R = 0.6268$, $p < 0.001$; o*Tbx1*$^{+/-}$, $R = 0.6491$, $p < 0.001$). The o*Tbx1*$^{+/+}$ and o*Tbx1*$^{+/-}$ mice did not differ in axon diameter range for g-ratios (genotype, p = 0.8131; genotype × axon diameter, p = 0.221). **C**. Average numbers (± SEM) of axons per image field versus axon diameter. The o*Tbx1*$^{+/+}$ and o*Tbx1*$^{+/-}$ mice differed ($\chi^2$ (27) = 109.7085, p = 6.22 × $10^{12}$) largely due to more axons of diameters ≥300nm and <800nm and fewer axons of ≥1,200nm and <1,500nm in o*Tbx1*$^{+/-}$ versus o*Tbx1*$^{+/+}$ mice, as determined by Mann-Whitney U tests applied to this diameter range (*, p < 0.05; **, p < 0.01; ***, p < 0.001; ****, p < 0.0001). The shift in axons toward small to medium sizes in o*Tbx1*$^{+/-}$ versus o*Tbx1*$^{+/+}$ mice resulted in a smaller average axon size for o*Tbx1*$^{+/-}$ mice versus o*Tbx1*$^{+/+}$ mice (Mann-Whitney non-parametric tests, p = 7.48 × $10^{19}$). **D**. Differences in the percentage of myelinated axons for o*Tbx1*$^{+/-}$ versus o*Tbx1*$^{+/+}$ mice versus axon diameter (Kolmogorov-Smirnov, p = 3.59 × $10^{16}$).

**Table S1. Primers used for genotyping**.

| Mouse line | Forward (5' → 3') | Reverse (5' → 3') | Purpose |
|---|---|---|---|
| *Pdgfrα-Cre* | olMR1084 (GCGGTCTGGCAGTAAAAACTATC) | olMR1085 (GTGAAACAGCATTGCTGTCACTT) | Generic cre - transgene |
| *Pdgfrα-Cre* | olMR7338 (CTAGGCCACAGAATTGAAAGATCT) | olMR7339 (GTAGGTGGAAATTCTAGCATCATCC) | Generic cre – internal positive control |
| *ROSA-CAG-tdTomato* | olMR9020 (AAGGGAGCTGCAGTGGAGTA) | olMR9021 (CCGAAAATCTGTGGGAAGTC) | tdTomato wild-type control |
| *ROSA-CAG-tdTomato* | olMR9103 (GGCATTAAAGCAGCGTATCC) | olMR9105 (CTGTTCCTGTACGGCATGG) | tdTomato mutant |
| *Tbx1*$^{+/flox}$ | 2g 1F (TCTTCTTGGGGCTGTAGACT) | Tbx1 1R (TGACTGTGCTGAAGTGCATC) | LoxP site |
| *Tbx1*$^{+/-}$ | KO1F (TTGGTGACGATCATCTCGGT) | KO1R (ATGATCTCCGCCGTGTCTAG) Mut2R (AGGTCCCTCGAAGAGGTTCA) | *Tbx1*$^{+/+}$ *Tbx1*$^{+/-}$ |

## References


Aguirre, A., & Gallo, V. (2004). Postnatal neurogenesis and gliogenesis in the olfactory bulb from NG2-expressing progenitors of the subventricular zone. *J Neurosci*, *24*(46), 10530–10541. https://doi.org/10.1523/JNEUROSCI.3572-04.2004

Alghamdi, M., Al Khalifah, R., Al Homyani, D. K., Alkhamis, W. H., Arold, S. T., Ekhzaimy, A., El-Wetidy, M., Kashour, T., & Halwani, R. (2020). A Novel TBX1 Variant Causing Hypoparathyroidism and Deafness. *J Endocr Soc*, *4*(2), bvz028. https://doi.org/10.1210/jendso/bvz028

Alhazmi, S., Alzahrani, M., Farsi, R., Alharbi, M., Algothmi, K., Alburae, N., Ganash, M., Azhari, S., Basingab, F., Almuhammadi, A., Alqosaibi, A., Alkhatabi, H., Elaimi, A., Jan, M., Aldhalaan, H. M., Alrafiah, A., & Alrofaidi, A. (2022). Multiple Recurrent Copy Number Variations (CNVs) in Chromosome 22 Including 22q11.2 Associated with Autism Spectrum Disorder. *Pharmgenomics Pers Med*, *15*, 705–720. https://doi.org/10.2147/PGPM.S366826

Allen Brain Atlas. (2017). Mouse Brain. *http://www.brain-map.org*.

Arbogast, T., Ouagazzal, A. M., Chevalier, C., Kopanitsa, M., Afinowi, N., Migliavacca, E., Cowling, B. S., Birling, M. C., Champy, M. F., Reymond, A., & Herault, Y. (2016). Reciprocal Effects on Neurocognitive and Metabolic Phenotypes in Mouse Models of 16p11.2 Deletion and Duplication Syndromes. *PLoS Genet*, *12*(2), e1005709. https://doi.org/10.1371/journal.pgen.1005709

Arnold, J. S., Werling, U., Braunstein, E. M., Liao, J., Nowotschin, S., Edelmann, W., Hebert, J. M., & Morrow, B. E. (2006). Inactivation of Tbx1 in the pharyngeal endoderm results in 22q11DS malformations. *Development*, *133*(5), 977–987. (Not in File)

Beiter, R. M., Rivet-Noor, C., Merchak, A. R., Bai, R., Johanson, D. M., Slogar, E., Sol-Church, K., Overall, C. C., & Gaultier, A. (2022). Evidence for oligodendrocyte progenitor cell heterogeneity in the adult mouse brain. *Sci Rep*, *12*(1), 12921. https://doi.org/10.1038/s41598-022-17081-7

Boku, S., Izumi, T., Abe, S., Takahashi, T., Nishi, A., Nomaru, H., Naka, Y., Kang, G., Nagashima, M., Hishimoto, A., Enomoto, S., Duran-Torres, G., Tanigaki, K., Zhang, J., Ye, K., Kato, S., Mannisto, P. T., Kobayashi, K., & Hiroi, N. (2018). Copy number elevation of 22q11.2 genes arrests the developmental maturation of working memory capacity and adult neurogenesis. *Molecular Psychiatry*, *23*(4), 985–992.

Bora, E., Lin, A., Wood, S. J., Yung, A. R., McGorry, P. D., & Pantelis, C. (2014). Cognitive deficits in youth with familial and clinical high risk to psychosis: a systematic review and meta-analysis. *Acta Psychiatr. Scand*, *130*(1), 1–15. (Not in File)

Brandebura, A. N., Morehead, M., Heller, D. T., Holcomb, P., Kolson, D. R., Jones, G., Mathers, P. H., & Spirou, G. A. (2018). Glial Cell Expansion Coincides with Neural Circuit Formation in the Developing Auditory Brainstem. *Dev Neurobiol*, *78*(11), 1097–1116. https://doi.org/10.1002/dneu.22633

Bronson, F. H., Dagg, C. P., & Snell, G. D. (2007). Reproduction. In E. L. Green (Ed.), *Biology of the Laboratory Mouse* (Second Edition ed., pp. Oneline publication). Dover Publications, Inc. (Reprinted from Not in File)

Caravella, K. E., & Roberts, J. E. (2017). Adaptive Skill Trajectories in Infants with Fragile X Syndrome Contrasted to Typical Controls and Infants at High Risk for Autism. *Res Autism Spectr Disord*, *40*, 1–12. https://doi.org/10.1016/j.rasd.2017.05.002

Ching, C. R. K., Gutman, B. A., Sun, D., Villalon Reina, J., Ragothaman, A., Isaev, D., Zavaliangos-Petropulu, A., Lin, A., Jonas, R. K., Kushan, L., Pacheco-Hansen, L., Vajdi, A., Forsyth, J. K., Jalbrzikowski, M., Bakker, G., van Amelsvoort, T., Antshel, K. M., Fremont, W., Kates, W. R.,...Bearden, C. E. (2020). Mapping Subcortical Brain Alterations in 22q11.2 Deletion

Syndrome: Effects of Deletion Size and Convergence With Idiopathic Neuropsychiatric Illness. *Am J Psychiatry*, *177*(7), 589–600. https://doi.org/10.1176/appi.ajp.2019.19060583

Chomiak, T., & Hu, B. (2009). What is the optimal value of the g-ratio for myelinated fibers in the rat CNS? A theoretical approach. *PLoS One*, *4*(11), e7754. https://doi.org/10.1371/journal.pone.0007754

de Vrij, F. M., Bouwkamp, C. G., Gunhanlar, N., Shpak, G., Lendemeijer, B., Baghdadi, M., Gopalakrishna, S., Ghazvini, M., Li, T. M., Quadri, M., Olgiati, S., Breedveld, G. J., Coesmans, M., Mientjes, E., de Wit, T., Verheijen, F. W., Beverloo, H. B., Cohen, D., Kok, R. M.,...Kushner, S. A. (2019). Candidate CSPG4 mutations and induced pluripotent stem cell modeling implicate oligodendrocyte progenitor cell dysfunction in familial schizophrenia. *Mol Psychiatry*, *24*, 757–771. https://doi.org/10.1038/s41380-017-0004-2

Di Giorgio, E., Rosa-Salva, O., Frasnelli, E., Calcagni, A., Lunghi, M., Scattoni, M. L., Simion, F., & Vallortigara, G. (2021). Abnormal visual attention to simple social stimuli in 4-month-old infants at high risk for Autism. *Sci Rep*, *11*(1), 15785. https://doi.org/10.1038/s41598-021-95418-4

Downes, N., & Mullins, P. (2014). The development of myelin in the brain of the juvenile rat. *Toxicol Pathol*, *42*(5), 913–922. https://doi.org/10.1177/0192623313503518

Eom, T. Y., Schmitt, J. E., Li, Y., Davenport, C. M., Steinberg, J., Bonnan, A., Alam, S., Ryu, Y. S., Paul, L., Hansen, B. S., Khairy, K., Pelletier, S., Pruett-Miller, S. M., Roalf, D. R., Gur, R. E., Emanuel, B. S., McDonald-McGinn, D. M., Smith, J. N., Li, C.,...Zakharenko, S. S. (2024). Tbx1 haploinsufficiency leads to local skull deformity, paraflocculus and flocculus dysplasia, and motor-learning deficit in 22q11.2 deletion syndrome. *Nat Commun*, *15*(1), 10510. https://doi.org/10.1038/s41467-024-54837-3

Esposito, G., Hiroi, N., & Scattoni, M. L. (2017). Cry, baby, cry: Expression of Distress as a Biomarker and Modulator in Autism Spectrum Disorder. *Int J Neuropsychopharmacol*, *20*(6), 498–503. https://doi.org/10.1093/ijnp/pyx014

Fejgin, K., Nielsen, J., Birknow, M. R., Bastlund, J. F., Nielsen, V., Lauridsen, J. B., Stefansson, H., Steinberg, S., Sorensen, H. B., Mortensen, T. E., Larsen, P. H., Klewe, I. V., Rasmussen, S. V., Stefansson, K., Werge, T. M., Kallunki, P., Christensen, K. V., & Didriksen, M. (2013). A Mouse Model that Recapitulates Cardinal Features of the 15q13.3 Microdeletion Syndrome Including Schizophrenia- and Epilepsy-Related Alterations. *Biol. Psychiatry*, *76*(2), 128–137. (Not in File)

Fonseca, A. H., Santana, G. M., Bosque Ortiz, G. M., Bampi, S., & Dietrich, M. O. (2021). Analysis of ultrasonic vocalizations from mice using computer vision and machine learning. *Elife*, *10*. https://doi.org/10.7554/eLife.59161

Fruttiger, M., Karlsson, L., Hall, A. C., Abramsson, A., Calver, A. R., Bostrom, H., Willetts, K., Bertold, C. H., Heath, J. K., Betsholtz, C., & Richardson, W. D. (1999). Defective oligodendrocyte development and severe hypomyelination in PDGF-A knockout mice. *Development*, *126*(3), 457–467.

Fuentealba, L. C., Rompani, S. B., Parraguez, J. I., Obernier, K., Romero, R., Cepko, C. L., & Alvarez-Buylla, A. (2015). Embryonic Origin of Postnatal Neural Stem Cells. *Cell*, *161*(7), 1644–1655. https://doi.org/10.1016/j.cell.2015.05.041

Gao, Z., Daquinag, A. C., Su, F., Snyder, B., & Kolonin, M. G. (2018). PDGFRalpha/PDGFRbeta signaling balance modulates progenitor cell differentiation into white and beige adipocytes. *Development*, *145*(1). https://doi.org/10.1242/dev.155861

Goh, S., Thiyagarajan, L., Dudding-Byth, T., Mark, P., & Kirk, E. P. (2024). A systematic review and pooled analysis of penetrance estimates of copy number variants associated with neurodevelopment. *Genet Med*, 101227. https://doi.org/10.1016/j.gim.2024.101227

Gong, W., Gottlieb, S., Collins, J., Blescia, A., Dietz, H., Goldmuntz, E., Donald-McGinn, D. M., Zackai, E. H., Emanuel, B. S., Driscoll, D. A., & Budarf, M. L. (2001). Mutation analysis of TBX1 in non-deleted patients with features of DGS/VCFS or isolated cardiovascular defects. *J. Med. Genet*, *38*(12), E45. (Not in File)

Gorny, J. H., Gorny, B., Wallace, D. G., & Whishaw, I. Q. (2002). Fimbria-fornix lesions disrupt the dead reckoning (homing) component of exploratory behavior in mice. *Learn Mem*, *9*(6), 387–394. https://doi.org/10.1101/lm.53002

Gur, R. C., Calkins, M. E., Satterthwaite, T. D., Ruparel, K., Bilker, W. B., Moore, T. M., Savitt, A. P., Hakonarson, H., & Gur, R. E. (2014). Neurocognitive growth charting in psychosis spectrum youths. *JAMA Psychiatry*, *71*(4), 366–374. (Not in File)

Gur, R. E., Yi, J. J., Donald-McGinn, D. M., Tang, S. X., Calkins, M. E., Whinna, D., Souders, M. C., Savitt, A., Zackai, E. H., Moberg, P. J., Emanuel, B. S., & Gur, R. C. (2014). Neurocognitive development in 22q11.2 deletion syndrome: comparison with youth having developmental delay and medical comorbidities. *Mol. Psychiatry*, *19*(11), 1205–1211. (Not in File)

Harper, K. M., Hiramoto, T., Tanigaki, K., Kang, G., Suzuki, G., Trimble, W., & Hiroi, N. (2012). Alterations of social interaction through genetic and environmental manipulation of the 22q11.2 gene Sept5 in the mouse brain. *Human Molecular Genetics*, *21*(15), 3489–3499. https://doi.org/10.1093/hmg/dds180

Hiramoto, T., Boku, S., Kang, G., Abe, S., Nagashima, M., Barbachan e Silva, M., O'Broin, P., Ye, K., Yamauchi, T., Michurin, T. V., Enikolopov, G., & Hiroi, N. (2023). Transcriptional regulation of neonatal neural stem cells is a determinant of social behavior. *bioRxiv*, *https://www.biorxiv.org/content/10.1101/2021.11.12.468452v2*.

Hiramoto, T., Kang, G., Suzuki, G., Satoh, Y., Kucherlapati, R., Watanabe, Y., & Hiroi, N. (2011). Tbx1: identification of a 22q11.2 gene as a risk factor for autism spectrum disorder in a mouse model. *Hum Mol Genet*, *20*(24), 4775–4785. https://doi.org/10.1093/hmg/ddr404

Hiramoto, T., Sumiyoshi, A., Kato, R., Yamauchi, T., Takano, T., Kang, G., Esparza, M., Matsumura, B., Stevens, L. J., Hiroi, Y. J., Tanifuji, T., Ryoke, R., Nonaka, H., Machida, A., Nomoto, K., Mogi, K., Kikusui, T., Kawashima, R., & Hiroi, N. (2025). Highly demarcated structural alterations in the brain and impaired social incentive learning in Tbx1 heterozygous mice. *Molecular Psychiatry*, *30*(https://www.nature.com/articles/s41380-024-02797-x), 1876–1886.

Hiramoto, T., Sumiyoshi, A., Yamauchi, T., Tanigaki, K., Shi, Q., Kang, G., Ryoke, R., Nonaka, H., Enomoto, S., Izumi, T., Bhat, M. A., Kawashima, R., & Hiroi, N. (2022). Tbx1, a gene encoded in 22q11.2 copy number variant, is a link between alterations in fimbria myelination and cognitive speed in mice. *Mol Psychiatry*, *27*(2), 929–938. https://doi.org/10.1038/s41380-021-01318-4

Hiroi, N. (2018). Critical Reappraisal of Mechanistic Links of Copy Number Variants to Dimensional Constructs of Neuropsychiatric Disorders in Mouse Models. *Psychiatry and Clinical Neurosciences*, *72*(5), 301–321.

Hiroi, N., Hiramoto, T., Harper, K. M., Suzuki, G., & Boku, S. (2012). Mouse models of 22q11.2-associated autism spectrum disorder. *Autism*, *S1*(001), 1–9. (In File)

Hiroi, N., & Nishi, A. (2015). Dimensional deconstruction and reconstruction of CNV-associated neuropsychiatric disorders. In M. V. Pletnikov & J. L. Waddington (Eds.), *Modeling the Psychopathological Dimensions of Schizophrenia: From Molecules to Behavior* (Vol. 23, pp. 285–302). (Reprinted from Not in File)

Hiroi, N., Takahashi, T., Hishimoto, A., Izumi, T., Boku, S., & Hiramoto, T. (2013). Copy Number Variation at 22q11.2: from rare variants to common mechanisms of developmental neuropsychiatric disorders. *Mol. Psychiatry*, *18*, 1153–1165. (Not in File)

Hiroi, N., & Yamauchi, T. (2019). Modeling and Predicting Developmental Trajectories of Neuropsychiatric Dimensions Associated With Copy Number Variations. *Int J Neuropsychopharmacol*, *22*(8), 488–500. https://doi.org/10.1093/ijnp/pyz026

Hiroi, N., Zhu, H., Lee, M., Funke, B., Arai, M., Itokawa, M., Kucherlapati, R., Morrow, B., Sawamura, T., & Agatsuma, S. (2005). A 200-kb region of human chromosome 22q11.2 confers antipsychotic-responsive behavioral abnormalities in mice. *Proceedings of the National Academy of Sciences of the United States of America*, *102*(52), 19132–19137. https://doi.org/10.1073/pnas.0509635102

Hodgetts, C. J., Stefani, M., Williams, A. N., Kolarik, B. S., Yonelinas, A. P., Ekstrom, A. D., Lawrence, A. D., Zhang, J., & Graham, K. S. (2020). The role of the fornix in human navigational learning. *Cortex*, *124*, 97–110. https://doi.org/10.1016/j.cortex.2019.10.017

Johansson, M., Hjarthag, F., & Helldin, L. (2020). Cognitive markers related to long-term remission status in Schizophrenia Spectrum Disorders. *Psychiatry Res*, *289*, 113035. https://doi.org/10.1016/j.psychres.2020.113035

Kaiser, T., Allen, H. M., Kwon, O., Barak, B., Wang, J., He, Z., Jiang, M., & Feng, G. (2021). MyelTracer: A Semi-Automated Software for Myelin g-Ratio Quantification. *eNeuro*, *8*(4). https://doi.org/10.1523/ENEURO.0558-20.2021

Kang, S. H., Fukaya, M., Yang, J. K., Rothstein, J. D., & Bergles, D. E. (2010). NG2+ CNS glial progenitors remain committed to the oligodendrocyte lineage in postnatal life and following neurodegeneration. *Neuron*, *68*(4), 668–681. https://doi.org/10.1016/j.neuron.2010.09.009

Kato, R., Machida, A., Nomoto, K., Kang, G., Hiramoto, T., Tanigaki, K., Mogi, K., Hiroi, N., & Kikusui, T. (2021). Maternal approach behaviors toward neonatal calls are impaired by mother's experiences of raising pups with a risk gene variant for autism. *Dev Psychobiol*, *63*(1), 108–113. https://doi.org/10.1002/dev.22006

Kelly, S., Jahanshad, N., Zalesky, A., Kochunov, P., Agartz, I., Alloza, C., Andreassen, O. A., Arango, C., Banaj, N., Bouix, S., Bousman, C. A., Brouwer, R. M., Bruggemann, J., Bustillo, J., Cahn, W., Calhoun, V., Cannon, D., Carr, V., Catts, S.,...Donohoe, G. (2018). Widespread white matter microstructural differences in schizophrenia across 4322 individuals: results from the ENIGMA Schizophrenia DTI Working Group. *Mol Psychiatry*, *23*(5), 1261–1269. https://doi.org/10.1038/mp.2017.170

Kendall, K. M., Rees, E., Escott-Price, V., Einon, M., Thomas, R., Hewitt, J., O'Donovan, M. C., Owen, M. J., Walters, J. T. R., & Kirov, G. (2017). Cognitive Performance Among Carriers of Pathogenic Copy Number Variants: Analysis of 152,000 UK Biobank Subjects. *Biol Psychiatry*, *82*(2), 103–110. https://doi.org/10.1016/j.biopsych.2016.08.014

Kochunov, P., Hong, L. E., Dennis, E. L., Morey, R. A., Tate, D. F., Wilde, E. A., Logue, M., Kelly, S., Donohoe, G., Favre, P., Houenou, J., Ching, C. R. K., Holleran, L., Andreassen, O. A., van Velzen, L. S., Schmaal, L., Villalon-Reina, J. E., Bearden, C. E., Piras, F.,...Jahanshad, N. (2020). ENIGMA-DTI: Translating reproducible white matter deficits into personalized vulnerability metrics in cross-diagnostic psychiatric research. *Hum Brain Mapp*, *43*(1), 194–206. https://doi.org/10.1002/hbm.24998

Komitova, M., Zhu, X., Serwanski, D. R., & Nishiyama, A. (2009). NG2 cells are distinct from neurogenic cells in the postnatal mouse subventricular zone. *J Comp Neurol*, *512*(5), 702–716. https://doi.org/10.1002/cne.21917

Koshiyama, D., Fukunaga, M., Okada, N., Morita, K., Nemoto, K., Usui, K., Yamamori, H., Yasuda, Y., Fujimoto, M., Kudo, N., Azechi, H., Watanabe, Y., Hashimoto, N., Narita, H., Kusumi, I., Ohi, K., Shimada, T., Kataoka, Y., Yamamoto, M.,...Cocoro. (2020). White matter microstructural alterations across four major psychiatric disorders: mega-analysis study in 2937 individuals. *Mol Psychiatry*, *25*(4), 883–895. https://doi.org/10.1038/s41380-019-0553-7

Liu, L., Ikonen, S., Heikkinen, T., Heikkila, M., Puolivali, J., van Groen, T., & Tanila, H. (2002). Effects of fimbria-fornix lesion and amyloid pathology on spatial learning and memory in transgenic APP+PS1 mice. *Behav Brain Res*, *134*(1-2), 433–445. https://doi.org/10.1016/s0166-4328(02)00058-x

Malhotra, D., & Sebat, J. (2012). CNVs: harbingers of a rare variant revolution in psychiatric genetics. *Cell*, *148*(6), 1223–1241. (Not in File)

Marcelin, G., Ferreira, A., Liu, Y., Atlan, M., Aron-Wisnewsky, J., Pelloux, V., Botbol, Y., Ambrosini, M., Fradet, M., Rouault, C., Henegar, C., Hulot, J. S., Poitou, C., Torcivia, A., Nail-Barthelemy, R., Bichet, J. C., Gautier, E. L., & Clement, K. (2017). A PDGFRalpha-Mediated Switch toward CD9(high) Adipocyte Progenitors Controls Obesity-Induced Adipose Tissue Fibrosis. *Cell Metab*, *25*(3), 673–685. https://doi.org/10.1016/j.cmet.2017.01.010

Marshall, C. R., Howrigan, D. P., Merico, D., Thiruvahindrapuram, B., Wu, W., Greer, D. S., Antaki, D., Shetty, A., Holmans, P. A., Pinto, D., Gujral, M., Brandler, W. M., Malhotra, D., Wang, Z., Fajarado, K. V. F., Maile, M. S., Ripke, S., Agartz, I., Albus, M.,...Schizophrenia Working Groups of the Psychiatric Genomics, C. (2017). Contribution of copy number variants to schizophrenia from a genome-wide study of 41,321 subjects. *Nat Genet*, *49*(1), 27–35. https://doi.org/10.1038/ng.3725

Matsuo, N., Takao, K., Nakanishi, K., Yamasaki, N., Tanda, K., & Miyakawa, T. (2010). Behavioral profiles of three C57BL/6 substrains. *Front Behav. Neurosci*, *4*, 29. (Not in File)

Meier, M. H., Caspi, A., Reichenberg, A., Keefe, R. S., Fisher, H. L., Harrington, H., Houts, R., Poulton, R., & Moffitt, T. E. (2014). Neuropsychological decline in schizophrenia from the premorbid to the postonset period: evidence from a population-representative longitudinal study. *Am. J. Psychiatry*, *171*(1), 91–101. (Not in File)

Menn, B., Garcia-Verdugo, J. M., Yaschine, C., Gonzalez-Perez, O., Rowitch, D., & Alvarez-Buylla, A. (2006). Origin of oligodendrocytes in the subventricular zone of the adult brain. *J Neurosci*, *26*(30), 7907–7918. https://doi.org/10.1523/JNEUROSCI.1299-06.2006

Michelini, G., Carlisi, C. O., Eaton, N. R., Elison, J. T., Haltigan, J. D., Kotov, R., Krueger, R. F., Latzman, R. D., Li, J. J., Levin-Aspenson, H. F., Salum, G. A., South, S. C., Stanton, K., Waldman, I. D., & Wilson, S. (2024). Where do neurodevelopmental conditions fit in transdiagnostic psychiatric frameworks? Incorporating a new neurodevelopmental spectrum. *World Psychiatry*, *23*(3), 333–357. https://doi.org/10.1002/wps.21225

Miller, M., Iosif, A. M., Hill, M., Young, G. S., Schwichtenberg, A. J., & Ozonoff, S. (2017). Response to Name in Infants Developing Autism Spectrum Disorder: A Prospective Study. *J Pediatr*, *183*, 141–146 e141. https://doi.org/10.1016/j.jpeds.2016.12.071

Miller, M., Sun, S., Iosif, A. M., Young, G. S., Belding, A., Tubbs, A., & Ozonoff, S. (2021). Repetitive behavior with objects in infants developing autism predicts diagnosis and later social behavior as early as 9 months. *J Abnorm Psychol*, *130*(6), 665–675. https://doi.org/10.1037/abn0000692

Misslin, R., Herzog, F., Koch, B., & Ropartz, P. (1982). Effects of isolation, handling and novelty on the pituitary--adrenal response in the mouse. *Psychoneuroendocrinology*, *7*(2-3), 217–221. (Not in File)

Nait Oumesmar, B., Vignais, L., & Baron-Van Evercooren, A. (1997). Developmental expression of platelet-derived growth factor alpha-receptor in neurons and glial cells of the mouse CNS. *J Neurosci*, *17*(1), 125–139. https://doi.org/10.1523/JNEUROSCI.17-01-00125.1997

Nakamura, M., Ye, K., MB, E. S., Yamauchi, T., Hoeppner, D. J., Fayyazuddin, A., Kang, G., Yuda, E. A., Nagashima, M., Enomoto, S., Hiramoto, T., Sharp, R., Kaneko, I., Tajinda, K., Adachi, M., Mihara, T., Tokuno, S., Geyer, M. A., Broin, P. O.,...Hiroi, N. (2021). Computational identification of variables in neonatal vocalizations predictive for postpubertal social

behaviors in a mouse model of 16p11.2 deletion. *Mol Psychiatry*, *26*(11), 6578–6588. https://doi.org/10.1038/s41380-021-01089-y

Nishi, A., & Hiroi, N. (2016). Genetic Mechanisms Emerging from Mouse Models of CNV-Associated Neuropsychiatric Disorders. In T. Abel & T. Nickl-Jockschat (Eds.), *The Neurobiology of Schizophrenia* (pp. 397–417). Academic Press/Elsevier. (Reprinted from Not in File)

Nishiyama, A., Lin, X. H., Giese, N., Heldin, C. H., & Stallcup, W. B. (1996). Co-localization of NG2 proteoglycan and PDGF alpha-receptor on O2A progenitor cells in the developing rat brain. *J Neurosci Res*, *43*(3), 299–314. https://doi.org/10.1002/(SICI)1097-4547(19960201)43:3<299::AID-JNR5>3.0.CO;2-E

Northrup, J. B., Leezenbaum, N. B., & Campbell, S. B. (2021). Observed Social Emotional Behavior at 22 Months Predicts a Later ASD Diagnosis in High-Risk Siblings. *J Autism Dev Disord*, *51*(9), 3187–3198. https://doi.org/10.1007/s10803-020-04789-6

O'Rourke, M., Cullen, C. L., Auderset, L., Pitman, K. A., Achatz, D., Gasperini, R., & Young, K. M. (2016). Evaluating Tissue-Specific Recombination in a Pdgfralpha-CreERT2 Transgenic Mouse Line. *PLoS One*, *11*(9), e0162858. https://doi.org/10.1371/journal.pone.0162858

Ogata, T., Niihori, T., Tanaka, N., Kawai, M., Nagashima, T., Funayama, R., Nakayama, K., Nakashima, S., Kato, F., Fukami, M., Aoki, Y., & Matsubara, Y. (2014). TBX1 mutation identified by exome sequencing in a Japanese family with 22q11.2 deletion syndrome-like craniofacial features and hypocalcemia. *PLoS. One*, *9*(3), e91598. (Not in File)

Olton, D. S., & Feustle, W. A. (1981). Hippocampal function required for nonspatial working memory. *Exp Brain Res*, *41*(3-4), 380–389. https://doi.org/10.1007/BF00238896

Owen, A. M., Roberts, A. C., Polkey, C. E., Sahakian, B. J., & Robbins, T. W. (1991). Extra-dimensional versus intra-dimensional set shifting performance following frontal lobe excisions, temporal lobe excisions or amygdalo-hippocampectomy in man. *Neuropsychologia*, *29*(10), 993–1006. (Not in File)

Ozonoff, S., Iosif, A. M., Baguio, F., Cook, I. C., Hill, M. M., Hutman, T., Rogers, S. J., Rozga, A., Sangha, S., Sigman, M., Steinfeld, M. B., & Young, G. S. (2010). A prospective study of the emergence of early behavioral signs of autism. *J. Am. Acad. Child Adolesc. Psychiatry*, *49*(3), 256–266. (Not in File)

Ozonoff, S., Young, G. S., Belding, A., Hill, M., Hill, A., Hutman, T., Johnson, S., Miller, M., Rogers, S. J., Schwichtenberg, A. J., Steinfeld, M., & Iosif, A. M. (2014). The broader autism phenotype in infancy: when does it emerge? *J. Am. Acad. Child Adolesc. Psychiatry*, *53*(4), 398–407. (Not in File)

Paylor, R., Glaser, B., Mupo, A., Ataliotis, P., Spencer, C., Sobotka, A., Sparks, C., Choi, C. H., Oghalai, J., Curran, S., Murphy, K. C., Monks, S., Williams, N., O'Donovan, M. C., Owen, M. J., Scambler, P. J., & Lindsay, E. (2006). Tbx1 haploinsufficiency is linked to behavioral disorders in mice and humans: implications for 22q11 deletion syndrome. *Proc. Natl. Acad. Sci. U. S. A*, *103*(20), 7729–7734. (Not in File)

Paylor, R., Spencer, C. M., Yuva-Paylor, L. A., & Pieke-Dahl, S. (2006). The use of behavioral test batteries, II: effect of test interval. *Physiol Behav*, *87*(1), 95–102. (Not in File)

Redmond, S. A., Figueres-Onate, M., Obernier, K., Nascimento, M. A., Parraguez, J. I., Lopez-Mascaraque, L., Fuentealba, L. C., & Alvarez-Buylla, A. (2019). Development of Ependymal and Postnatal Neural Stem Cells and Their Origin from a Common Embryonic Progenitor. *Cell Rep*, *27*(2), 429–441 e423. https://doi.org/10.1016/j.celrep.2019.01.088

Rivers, L. E., Young, K. M., Rizzi, M., Jamen, F., Psachoulia, K., Wade, A., Kessaris, N., & Richardson, W. D. (2008). PDGFRA/NG2 glia generate myelinating oligodendrocytes and piriform projection neurons in adult mice. *Nat Neurosci*, *11*(12), 1392–1401. https://doi.org/10.1038/nn.2220

Rushing, G., & Ihrie, R. A. (2016). Neural stem cell heterogeneity through time and space in the ventricular-subventricular zone. *Front Biol (Beijing)*, *11*(4), 261–284. https://doi.org/10.1007/s11515-016-1407-1

Saito, R., Koebis, M., Nagai, T., Shimizu, K., Liao, J., Wulaer, B., Sugaya, Y., Nagahama, K., Uesaka, N., Kushima, I., Mori, D., Maruyama, K., Nakao, K., Kurihara, H., Yamada, K., Kano, M., Fukada, Y., Ozaki, N., & Aiba, A. (2020). Comprehensive analysis of a novel mouse model of the 22q11.2 deletion syndrome: a model with the most common 3.0-Mb deletion at the human 22q11.2 locus. *Transl Psychiatry*, *10*(1), 35. https://doi.org/10.1038/s41398-020-0723-z

Sakamoto, Y., Takano, T., Shimoyama, S., Hiramoto, T., Hiroi, N., & Nakamura, K. (2025). Prepartum bumetanide treatment reverses altered neonatal social communication but non-specifically reduces post-pubertal social behavior in a mouse model of fragile X syndrome. *Genomic Psychiatry*, *1*(1), 61–72. (In File)

Schneider, M., Debbane, M., Bassett, A. S., Chow, E. W., Fung, W. L., van den Bree, M., Owen, M., Murphy, K. C., Niarchou, M., Kates, W. R., Antshel, K. M., Fremont, W., McDonald-McGinn, D. M., Gur, R. E., Zackai, E. H., Vorstman, J., Duijff, S. N., Klaassen, P. W., Swillen, A.,...Behavior in 22q11.2 Deletion, S. (2014). Psychiatric disorders from childhood to adulthood in 22q11.2 deletion syndrome: results from the International Consortium on Brain and Behavior in 22q11.2 Deletion Syndrome. *Am J Psychiatry*, *171*(6), 627–639. https://doi.org/10.1176/appi.ajp.2013.13070864

Seidman, L. J., Shapiro, D. I., Stone, W. S., Woodberry, K. A., Ronzio, A., Cornblatt, B. A., Addington, J., Bearden, C. E., Cadenhead, K. S., Cannon, T. D., Mathalon, D. H., McGlashan, T. H., Perkins, D. O., Tsuang, M. T., Walker, E. F., & Woods, S. W. (2016). Association of Neurocognition With Transition to Psychosis: Baseline Functioning in the Second Phase of the North American Prodrome Longitudinal Study. *JAMA Psychiatry*, *73*(12), 1239–1248. https://doi.org/10.1001/jamapsychiatry.2016.2479

Sheffield, J. M., Karcher, N. R., & Barch, D. M. (2018). Cognitive Deficits in Psychotic Disorders: A Lifespan Perspective. *Neuropsychol Rev*, *28*(4), 509–533. https://doi.org/10.1007/s11065-018-9388-2

Sil, S., Periyasamy, P., Thangaraj, A., Chivero, E. T., & Buch, S. (2018). PDGF/PDGFR axis in the neural systems. *Mol Aspects Med*, *62*, 63–74. https://doi.org/10.1016/j.mam.2018.01.006

Simon, M. M., Greenaway, S., White, J. K., Fuchs, H., Gailus-Durner, V., Wells, S., Sorg, T., Wong, K., Bedu, E., Cartwright, E. J., Dacquin, R., Djebali, S., Estabel, J., Graw, J., Ingham, N. J., Jackson, I. J., Lengeling, A., Mandillo, S., Marvel, J.,...Brown, S. D. (2013). A comparative phenotypic and genomic analysis of C57BL/6J and C57BL/6N mouse strains. *Genome Biol*, *14*(7), R82. (Not in File)

Singh, T., Poterba, T., Curtis, D., Akil, H., Al Eissa, M., Barchas, J. D., Bass, N., Bigdeli, T. B., Breen, G., Bromet, E. J., Buckley, P. F., Bunney, W. E., Bybjerg-Grauholm, J., Byerley, W. F., Chapman, S. B., Chen, W. J., Churchhouse, C., Craddock, N., Cusick, C. M.,...Daly, M. J. (2022). Rare coding variants in ten genes confer substantial risk for schizophrenia. *Nature*, *604*(7906), 509–516. https://doi.org/10.1038/s41586-022-04556-w

Sonderby, I. E., Ching, C. R. K., Thomopoulos, S. I., van der Meer, D., Sun, D., Villalon-Reina, J. E., Agartz, I., Amunts, K., Arango, C., Armstrong, N. J., Ayesa-Arriola, R., Bakker, G., Bassett, A. S., Boomsma, D. I., Bulow, R., Butcher, N. J., Calhoun, V. D., Caspers, S., Chow, E. W. C.,...Group, E. q. D. S. W. (2021). Effects of copy number variations on brain structure and risk for psychiatric illness: Large-scale studies from the ENIGMA working groups on CNVs. *Hum Brain Mapp*. https://doi.org/10.1002/hbm.25354

Stefansson, H., Meyer-Lindenberg, A., Steinberg, S., Magnusdottir, B., Morgen, K., Arnarsdottir, S., Bjornsdottir, G., Walters, G. B., Jonsdottir, G. A., Doyle, O. M., Tost, H., Grimm, O.,

Kristjansdottir, S., Snorrason, H., Davidsdottir, S. R., Gudmundsson, L. J., Jonsson, G. F., Stefansdottir, B., Helgadottir, I.,...Stefansson, K. (2014). CNVs conferring risk of autism or schizophrenia affect cognition in controls. *Nature*, *505*(7483), 361–366. https://doi.org/10.1038/nature12818

Sun, D., Ching, C. R. K., Lin, A., Forsyth, J. K., Kushan, L., Vajdi, A., Jalbrzikowski, M., Hansen, L., Villalon-Reina, J. E., Qu, X., Jonas, R. K., van Amelsvoort, T., Bakker, G., Kates, W. R., Antshel, K. M., Fremont, W., Campbell, L. E., McCabe, K. L., Daly, E.,...Bearden, C. E. (2020). Large-scale mapping of cortical alterations in 22q11.2 deletion syndrome: Convergence with idiopathic psychosis and effects of deletion size. *Mol Psychiatry*, *25*(8), 1822–1834. https://doi.org/10.1038/s41380-018-0078-5

Sung, S., Fenoglio, A., Wolff, J. J., Schultz, R. T., Botteron, K. N., Dager, S. R., Estes, A. M., Hazlett, H. C., Zwaigenbaum, L., Piven, J., Elison, J. T., & Network, I. (2022). Examining the factor structure and discriminative utility of the Infant Behavior Questionnaire-Revised in infant siblings of autistic children. *Child Dev*, *93*(5), 1398–1413. https://doi.org/10.1111/cdev.13781

Suzuki, G., Harper, K. M., Hiramoto, T., Funke, B., Lee, M., Kang, G., Buell, M., Geyer, M. A., Kucherlapati, R., Morrow, B., Mannisto, P. T., Agatsuma, S., & Hiroi, N. (2009). Over-expression of a human chromosome 22q11.2 segment including TXNRD2, COMT and ARVCF developmentally affects incentive learning and working memory in mice. *Human Molecular Genetics*, *18*(20), 3914–3925. https://doi.org/10.1093/hmg/ddp334

Suzuki, G., Harper, K. M., Hiramoto, T., Sawamura, T., Lee, M., Kang, G., Tanigaki, K., Buell, M., Geyer, M. A., Trimble, W. S., Agatsuma, S., & Hiroi, N. (2009). Sept5 deficiency exerts pleiotropic influence on affective behaviors and cognitive functions in mice. *Human Molecular Genetics*, *18*(9), 1652–1660. https://doi.org/10.1093/hmg/ddp086

Takahashi, T., Okabe, S., Broin, P. O., Nishi, A., Ye, K., Beckert, M. V., Izumi, T., Machida, A., Kang, G., Abe, S., Pena, J. L., Golden, A., Kikusui, T., & Hiroi, N. (2016). Structure and function of neonatal social communication in a genetic mouse model of autism. *Mol Psychiatry*, *21*(9), 1208–1214. https://doi.org/10.1038/mp.2015.190

Thompson, C. L., Ng, L., Menon, V., Martinez, S., Lee, C. K., Glattfelder, K., Sunkin, S. M., Henry, A., Lau, C., Dang, C., Garcia-Lopez, R., Martinez-Ferre, A., Pombero, A., Rubenstein, J. L. R., Wakeman, W. B., Hohmann, J., Dee, N., Sodt, A. J., Young, R.,...Jones, A. R. (2014). A high-resolution spatiotemporal atlas of gene expression of the developing mouse brain. *Neuron*, *83*(2), 309–323. https://doi.org/10.1016/j.neuron.2014.05.033

Thompson, P. M., Jahanshad, N., Ching, C. R. K., Salminen, L. E., Thomopoulos, S. I., Bright, J., Baune, B. T., Bertolin, S., Bralten, J., Bruin, W. B., Bulow, R., Chen, J., Chye, Y., Dannlowski, U., de Kovel, C. G. F., Donohoe, G., Eyler, L. T., Faraone, S. V., Favre, P.,...Consortium, E. (2020). ENIGMA and global neuroscience: A decade of large-scale studies of the brain in health and disease across more than 40 countries. *Transl Psychiatry*, *10*(1), 100. https://doi.org/10.1038/s41398-020-0705-1

Tripathi, R. B., Rivers, L. E., Young, K. M., Jamen, F., & Richardson, W. D. (2010). NG2 glia generate new oligodendrocytes but few astrocytes in a murine experimental autoimmune encephalomyelitis model of demyelinating disease. *J Neurosci*, *30*(48), 16383–16390. https://doi.org/10.1523/JNEUROSCI.3411-10.2010

Tschentscher, N., Woll, C. F. J., Tafelmaier, J. C., Kriesche, D., Bucher, J. C., Engel, R. R., & Karch, S. (2023). Neurocognitive Deficits in First-Episode and Chronic Psychotic Disorders: A Systematic Review from 2009 to 2022. *Brain Sci*, *13*(2). https://doi.org/10.3390/brainsci13020299

Villalon-Reina, J. E., Martinez, K., Qu, X., Ching, C. R. K., Nir, T. M., Kothapalli, D., Corbin, C., Sun, D., Lin, A., Forsyth, J. K., Kushan, L., Vajdi, A., Jalbrzikowski, M., Hansen, L., Jonas, R. K., van

Amelsvoort, T., Bakker, G., Kates, W. R., Antshel, K. M.,...Bearden, C. E. (2020). Altered white matter microstructure in 22q11.2 deletion syndrome: a multisite diffusion tensor imaging study. *Mol Psychiatry*, *25*(11), 2818–2831. https://doi.org/10.1038/s41380-019-0450-0

White, N. M., & McDonald, R. J. (2002). Multiple parallel memory systems in the brain of the rat. *Neurobiol Learn Mem*, *77*(2), 125–184. https://doi.org/10.1006/nlme.2001.4008

Yamauchi, T., Kang, G., & Hiroi, N. (2020a). Heterozygosity of murine Crkl does not recapitulate behavioral dimensions of human 22q11.2 hemizygosity. *Genes Brain and Behavior*, *20*(5), e12719. https://doi.org/https://doi.org/10.1111/gbb.12719

Yamauchi, T., Kang, G., & Hiroi, N. (2020b). Heterozygosity of murine Crkl does not recapitulate behavioral dimensions of human 22q11.2 hemizygosity. *Genes Brain Behav*, e12719. https://doi.org/10.1111/gbb.12719

Yang, D., Wang, Y., Qi, T., Zhang, X., Shen, L., Ma, J., Pang, Z., Lal, N. K., McClatchy, D. B., Seradj, S. H., Leung, V. H., Wang, K., Xie, Y., Polli, F. S., Maximov, A., Gonzalez, O. C., de Lecea, L., Cline, H. T., Augustine, V.,...Ye, L. (2024). Phosphorylation of pyruvate dehydrogenase inversely associates with neuronal activity. *Neuron*, *112*(6), 959–971 e958. https://doi.org/10.1016/j.neuron.2023.12.015

Zhu, H., Lee, M., Agatsuma, S., & Hiroi, N. (2007). Pleiotropic impact of constitutive fosB inactivation on nicotine-induced behavioral alterations and stress-related traits in mice. *Human Molecular Genetics*, *16*(7), 820–836. https://doi.org/10.1093/hmg/ddm027

Zhu, X., Bergles, D. E., & Nishiyama, A. (2008). NG2 cells generate both oligodendrocytes and gray matter astrocytes. *Development*, *135*(1), 145–157. https://doi.org/10.1242/dev.004895

Zhu, X., Hill, R. A., & Nishiyama, A. (2008). NG2 cells generate oligodendrocytes and gray matter astrocytes in the spinal cord. *Neuron Glia Biol*, *4*(1), 19–26. https://doi.org/10.1017/S1740925X09000015

Zinkstok, J., Boot, E., Bassett, A. S., Hiroi, N., Butcher, N. J., Vingerhoets, C., Vorstman, J. A. S., & van Amelsvoort, T. A. M. J. (2019). The 22q11.2 deletion syndrome from a neurobiological perspective. *Lancet Psychiatry*, *6*(11), 951–960. https://doi.org/10.1016/S2215-0366(19)30076-8

**Figure 1**

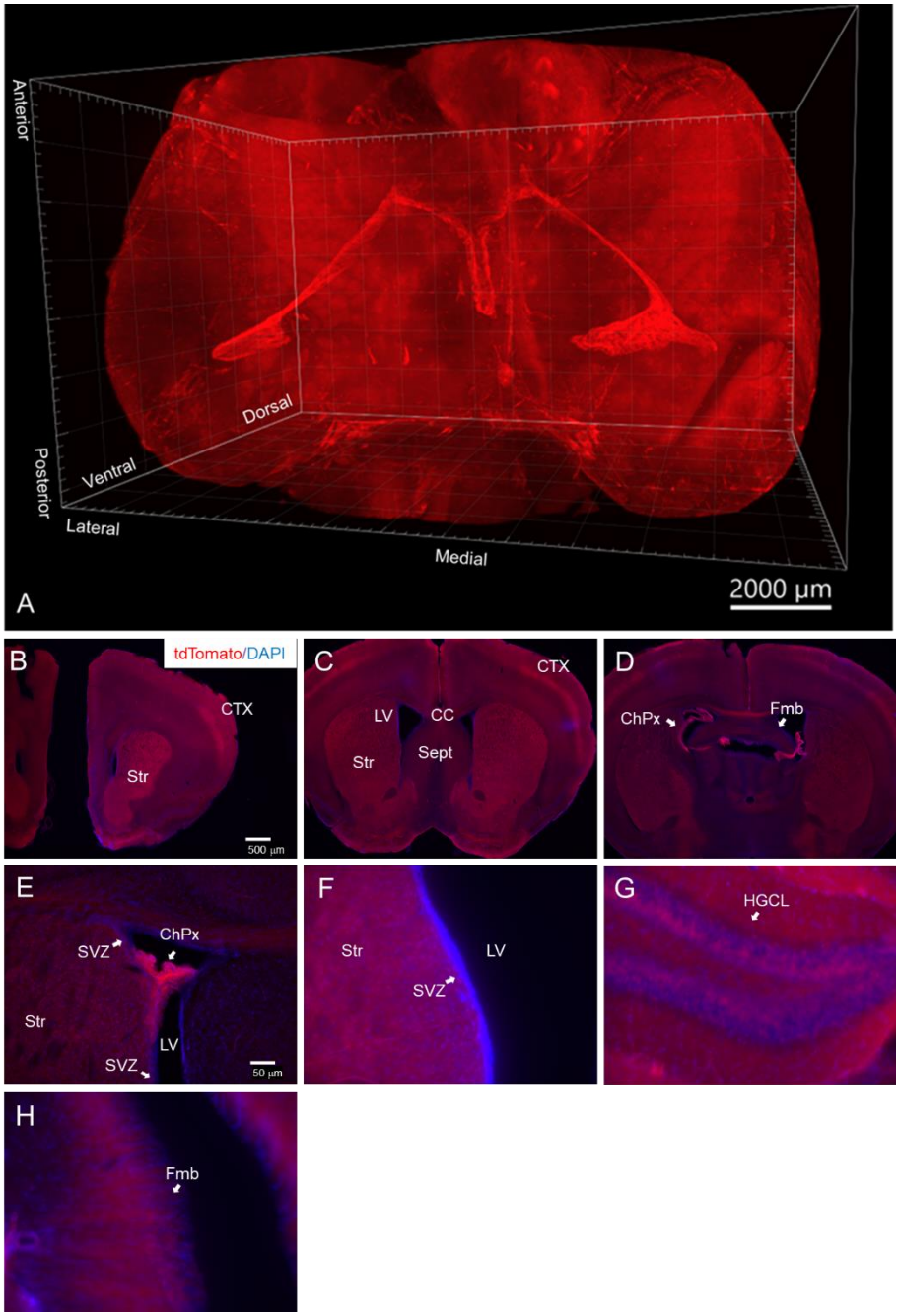
Anterior
Posterior
Dorsal
Ventral
Lateral
Medial
2000 µm
A
B
tdTomato/DAPI
CTX
Str
500 µm
C
CTX
LV
CC
Str
Sept
D
ChPx
Fmb
E
SVZ
ChPx
Str
LV
SVZ
50 µm
F
Str
LV
SVZ
G
HGCL
H
Fmb

**Figure 2**

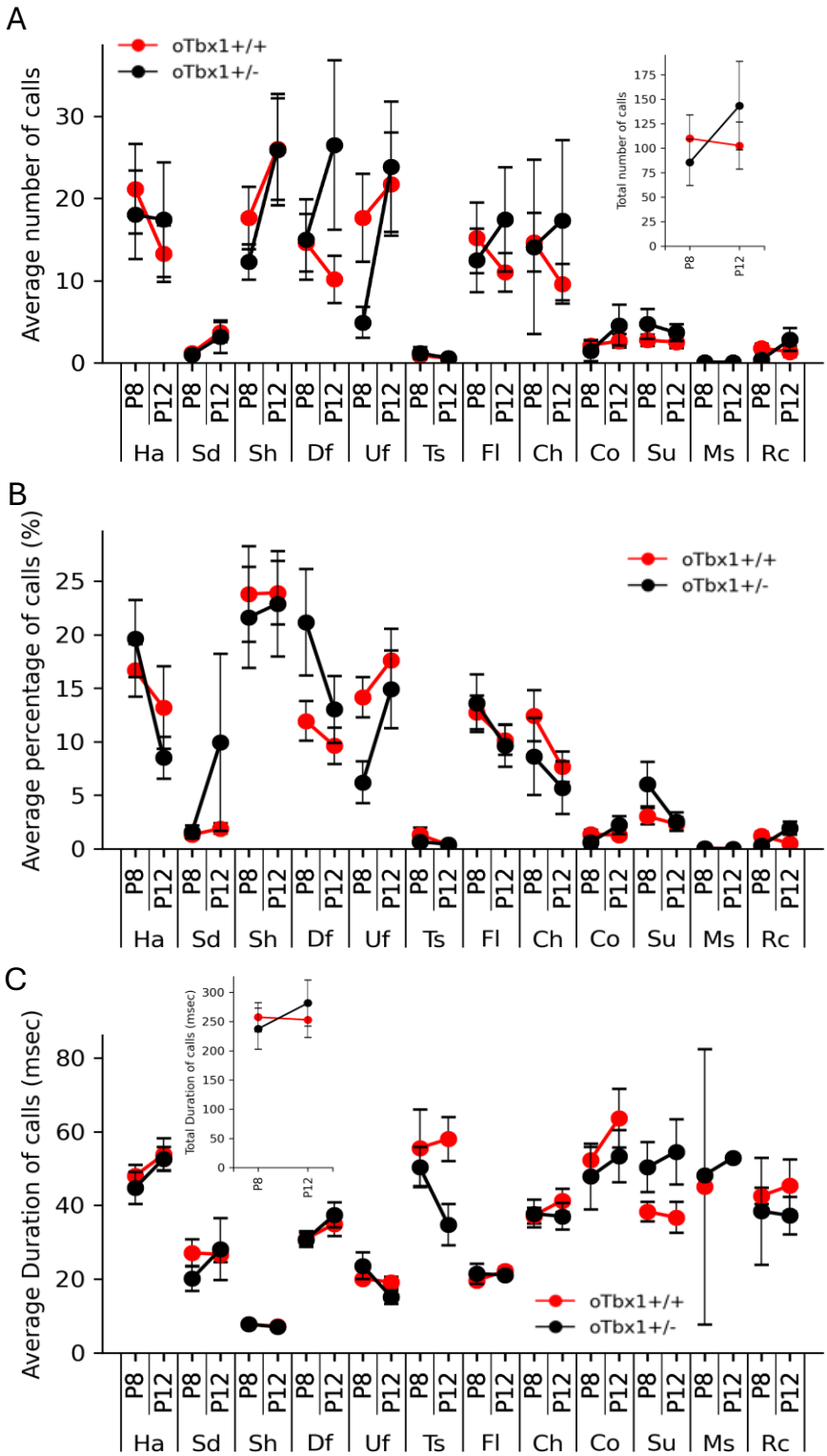
A
oTbx1+/+
oTbx1+/-
Average number of calls
Total number of calls
P8
P12
Ha
Sd
Sh
Df
Uf
Ts
Fl
Ch
Co
Su
Ms
Rc
B
Average percentage of calls (%)
C
Average Duration of calls (msec)
Total Duration of calls (msec)

**Figure 3**

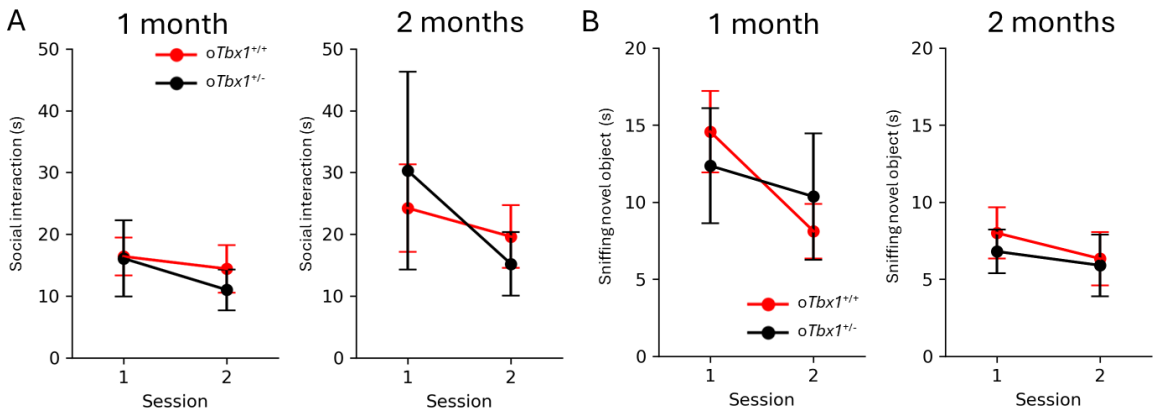


**Figure 4**

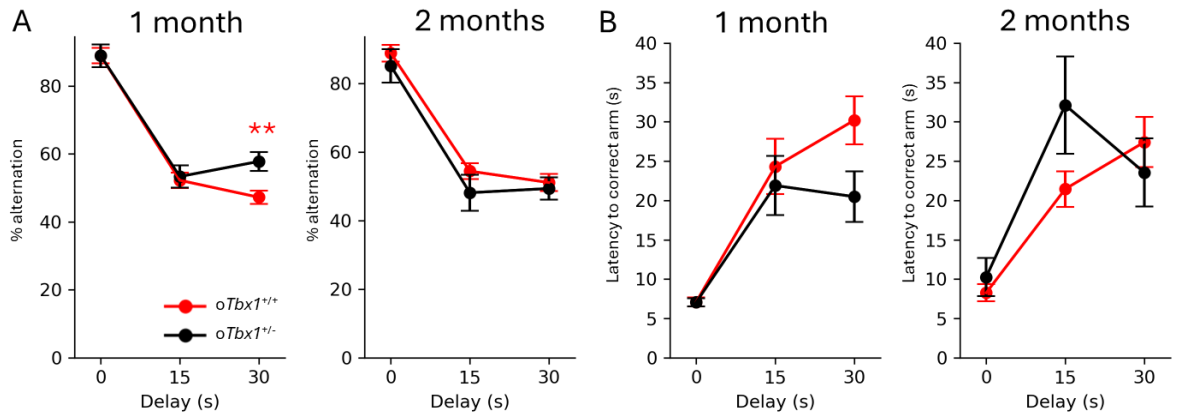


**Figure 5**

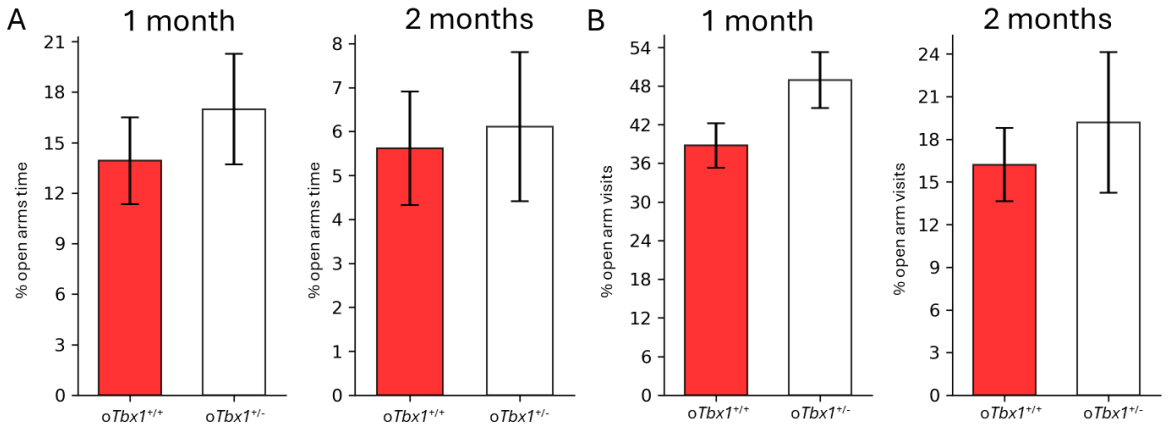

**Figure 6**

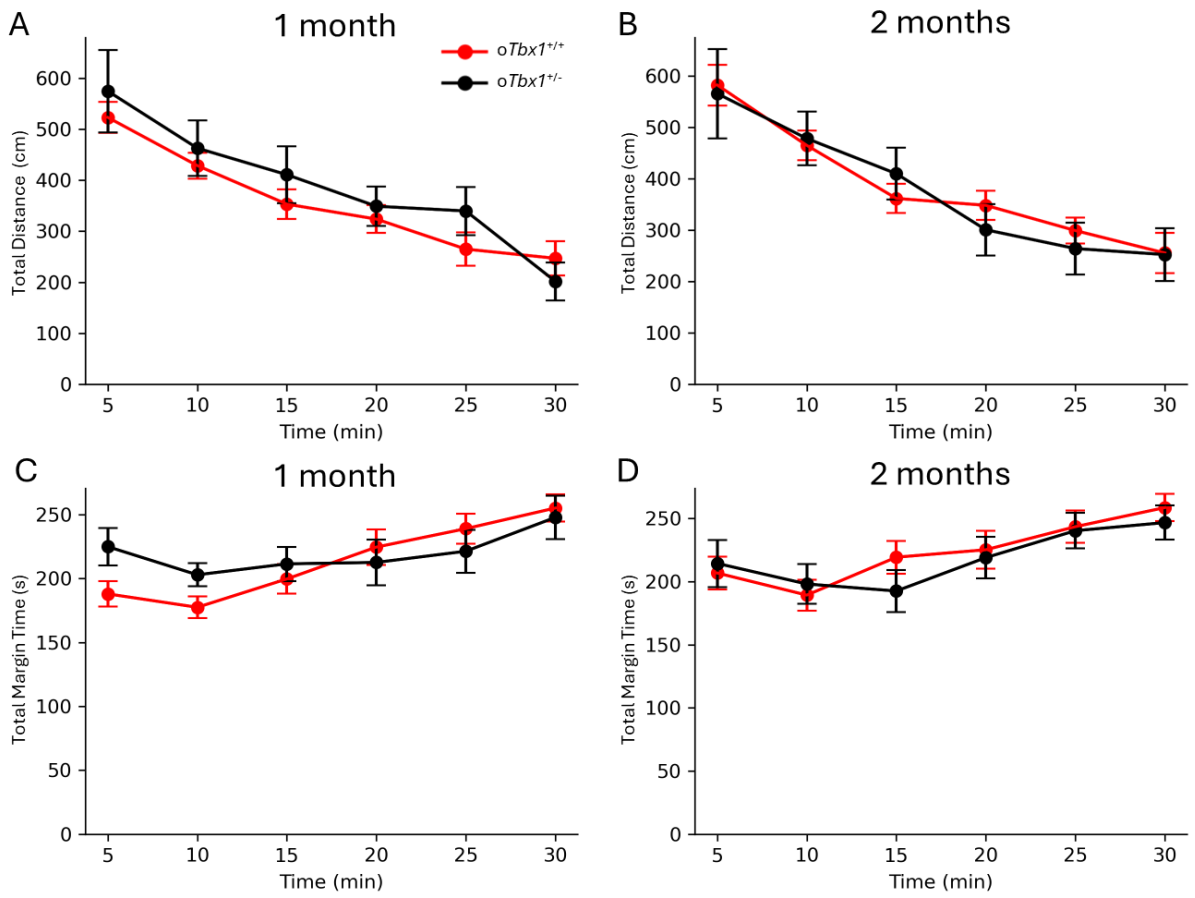
A
1 month
oTbx1+/+
oTbx1+/-
Total Distance (cm)
Time (min)
B
2 months
Total Distance (cm)
Time (min)
C
1 month
Total Margin Time (s)
Time (min)
D
2 months
Total Margin Time (s)
Time (min)

**Figure 7**

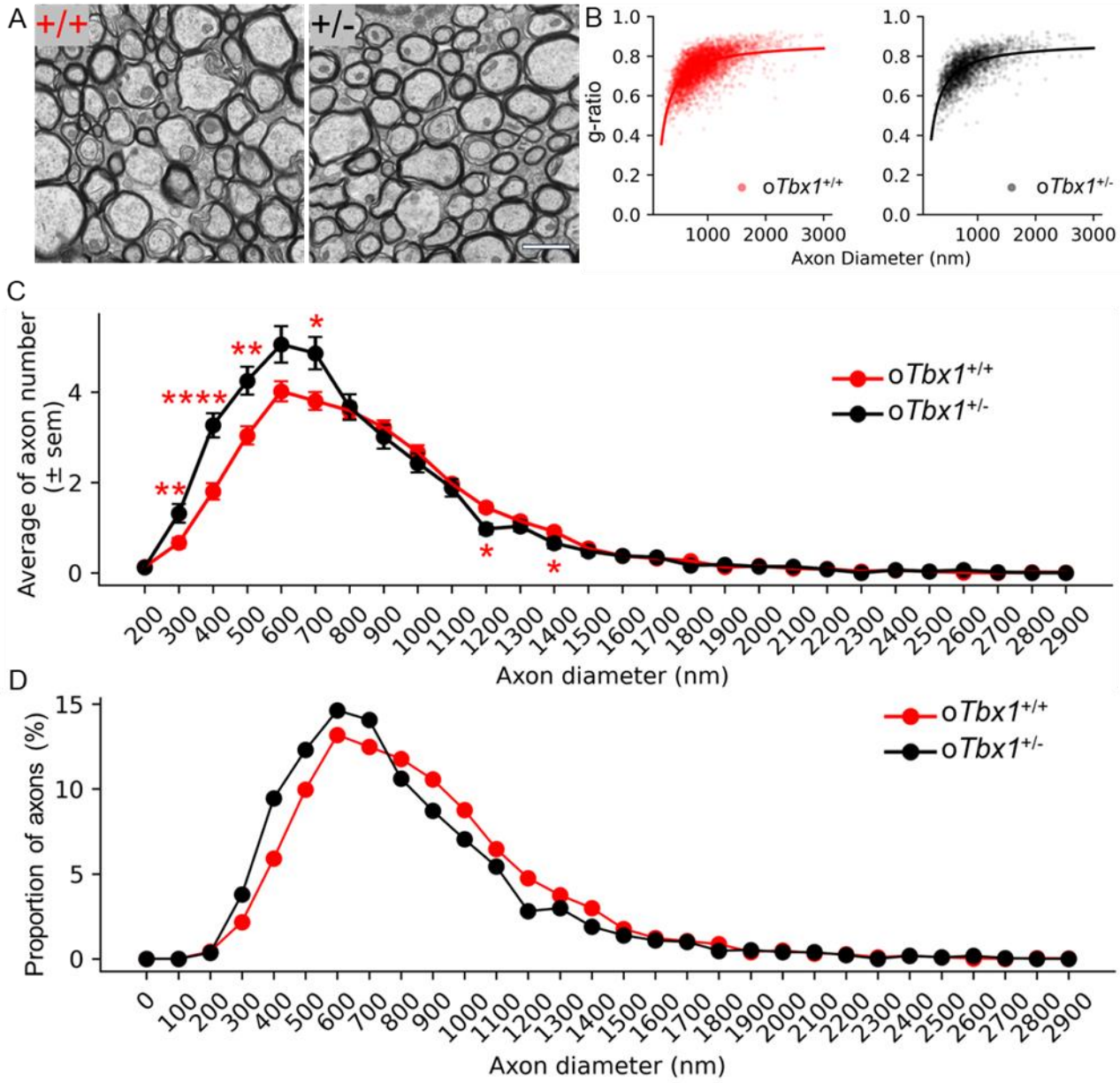
A
+/+
+/-
B
g-ratio
1.0
0.8
0.6
0.4
0.2
0.0
1000 2000 3000
Axon Diameter (nm)
oTbx1+/+
oTbx1+/-
C
Average of axon number (± sem)
Axon diameter (nm)
oTbx1+/+
oTbx1+/-
D
Proportion of axons (%)
Axon diameter (nm)
oTbx1+/+
oTbx1+/-

**Supplementary Information**

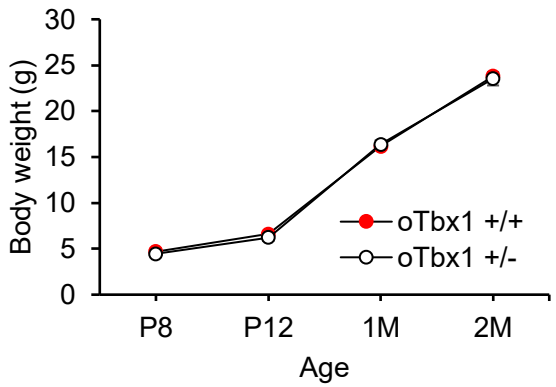


**Figure S1.** Body weights o*Tbx1*$^{+/+}$ and o*Tbx1*$^{+/-}$ mice. o*Tbx1*$^{+/+}$ and o*Tbx1*$^{+/-}$ mice had indistinguishable body weight increases from P8 to 2 months of age (P8, U = 115.5, p = 0.5681; P12, U = 132, p = 0.3685; 1 month, U = 161.5, p = 0.687; U = 102, p = 0.9158). o*Tbx1*$^{+/+}$ P8, N = 24, P12; N = 27; 1 month, N = 27; 2 months, N = 21: o*Tbx1*$^{+/-}$: P8, N = 11, P12, N = 12; 1 month, N = 11; 2 months, N = 10.

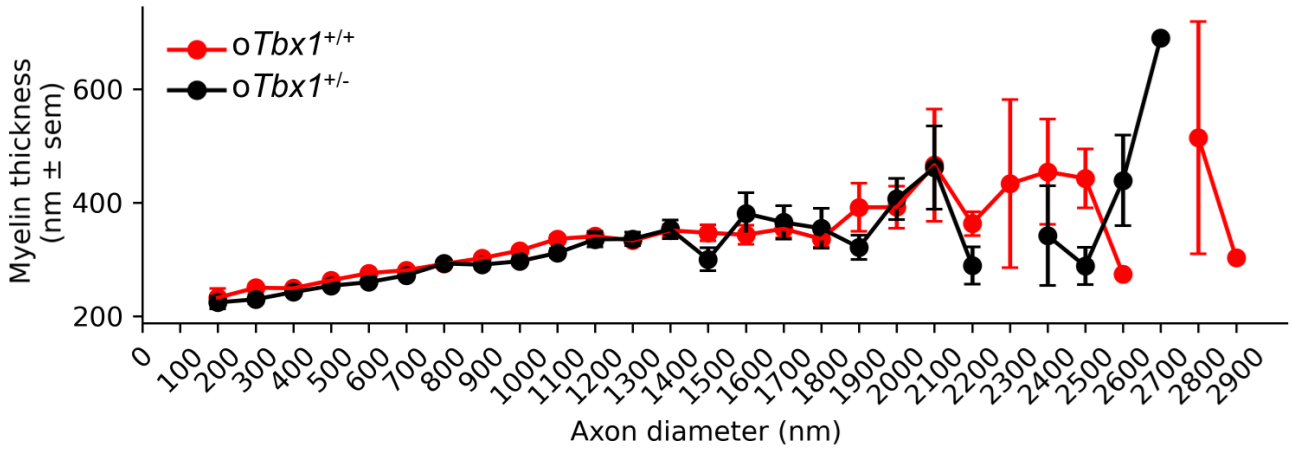


**Supplementary Figure S2.** The myelin thickness of axons for o*Tbx1*$^{+/-}$ versus o*Tbx1*$^{+/+}$ mice versus axon diameter was similar along the axon diameter range (genotype, p = 0.931; genotype × axon diameter, p = 0.814).